CHALMERS
UNIVERSITY OF TECHNOLOGY

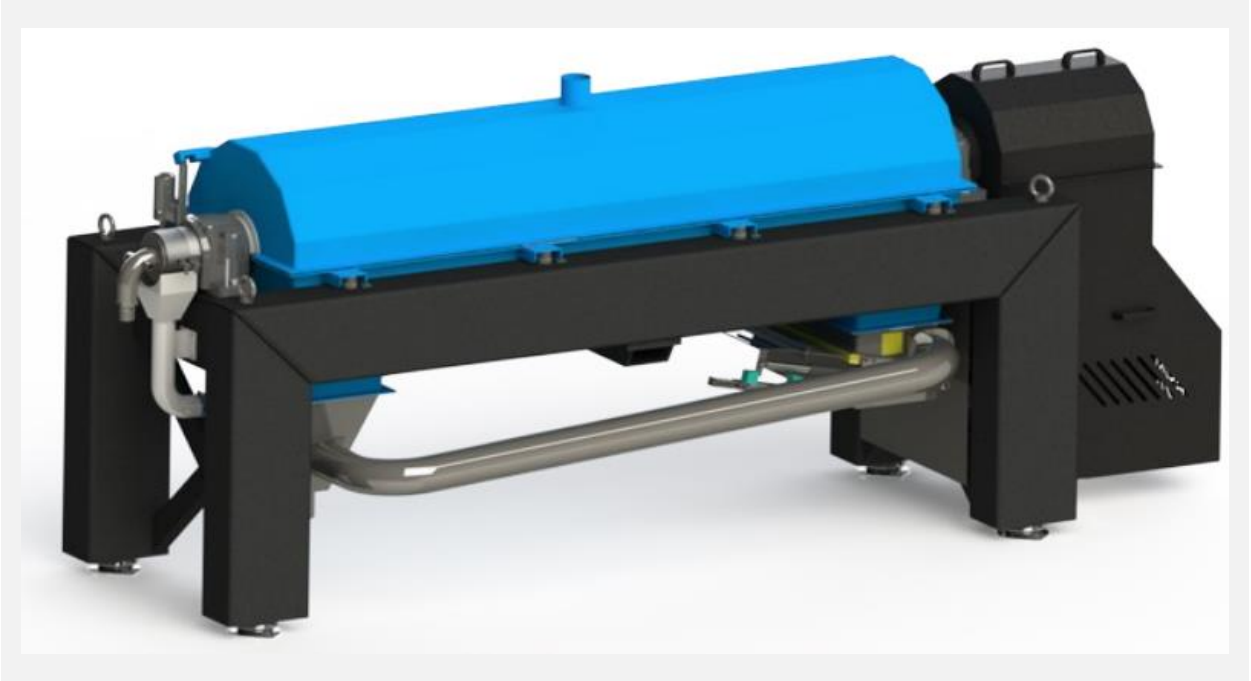

CFD Applied to Decanter Centrifuges

Master's thesis in Applied Mechanics

Anirudh Bhat

DEPARTMENT OF MECHANICS AND
MARITIME SCIENCES

CHALMERS UNIVERSITY OF TECHNOLOGY
Gothenburg, Sweden 2022
www.chalmers.se

MASTER'S THESIS IN APPLIED MECHANICS

CFD Applied to Decanter Centrifuges

ANIRUDH BHAT

Department of Mechanics and Maritime Sciences
Division of Fluid dynamics
CHALMERS UNIVERSITY OF TECHNOLOGY
Göteborg, Sweden 2022

CFD Applied to Decanter Centrifuges
ANIRUDH BHAT

Master's thesis 2022:61
Department of Mechanics and Maritime Sciences
Division of Fluid dynamics
Chalmers University of Technology
SE-412 96 Göteborg
Sweden
Telephone: +46 (0)31-772 1000

Typeset in LaTeX
Göteborg, Sweden 2022

CFD Applied to Decanter Centrifuges
Master's thesis in Applied Mechanics
ANIRUDH BHAT
Department of Mechanics and Maritime Sciences
Division of Fluid dynamics
Chalmers University of Technology

Abstract

Decanter centrifuges have become a crucial part of numerous industrial solid-liquid separation processes. Its use in dewatering of municipal sewage slurries has made it an immensely valuable tool in combating water pollution. The flow and separation of various phases through a decanter centrifuge can be influenced by a host of parameters such as the slurry rheology, the solid phase size distribution, and operational parameters of the the operation such as the mass flow rate of the slurry through the machine, geometrical design features of the centrifuge and many more. The development of a feasible and reliable computational model would facilitate the qualitative testing of the influence of many of these parameters on the performance of the decanter without relying on expensive experimental tests.

In this project, computational fluid dynaimcs (CFD) has been used to model the flow of municipal sewage slurry within a decanter centrifuge. A sliding mesh approach was used to model the rotation of the decanter centrifuge and a moving wall boundary condition is applied to the surface of the centrifuge drum to simulate the speed differential. The multiphase flow equations were solved by using the Eulerian mixture multiphase model by modelling the slurry as a two phase mixture of water and the heavier phase to be separated wherein the heavier phase is modelled as a relatively thick and viscous liquid. Direct validation of the developed model against experimental data was not feasible, but a qualitative judgement about the model was made based on the literature survey and the insights provided by the decanter centrifuge manufacturer. Four test cases were run on the developed model to test how it reacts to a change in certain parameters. Three of the cases test the effect of varying the heavier phase's viscosity and the fourth case tests the model at a higher inlet mass flow rate.

Keywords: Decanter centrifuge, dewatering, Sewage sludge, CFD, Mixture multiphase

Preface

The work presented in this report summarizes the work conducted by Anirudh Bhat for their master's thesis towards a Master's degree in Applied Mechanics at Chalmers Univesity of Technology, Gothenburg. The thesis work was carried out at Semcon Sweden AB in cooperation with Noxon AB with Federico Ghirelli as the supervisor and Professor Srdjan Sasic as the examiner. The thesis was opposed by Erik Döhler at Chalmers Unviersity of Technology.

Acknowledgements

I would like to extend my gratitude towards all the people involved in making this project possible. Firstly, I would like to thank my supervisor at Semcon Sweden AB, Federico Ghirelli who helped me at every stage of this project by providing valuable input and feedback for my work. Even in the face of the numerous challenges faced by the project, he has been a great support and an excellent guide. Next, I would like to Professor Srdjan Sasic not only for being my examiner for the master's theis but also for imparting his knowledge and showing a way forward whenever complications were encountered in the project and it was a great pleasure to have discussions with him. Next, I would like to thank Fredrik Carlsson, who gave me the opportunity work on this challenging project in the first place. He help was valuable in sorting out many of the technical difficulties that we encountered throughout the course of this project. Finally I would also like to thank Robin Victor at Volupe for providing guidance with many technical queries pertaining to Star-CCM+.

I would also like to thank Martin Evebron and Magnus Johansson from Noxon AB for providing all the necessary details about decanter centrifuges, which proved to be invaluable in setting up the project.

Nomenclature

Variables

Δt	Time-step	$[s]$
$\dot{m}$	Mass flow rate	$[kg/s]$
$\mathbf{a}$	Area vector	$[m^2]$
$\mathbf{I}$	Identity matrix	$[-]$
$\mathbf{J}^{\phi}$	Face flux of variable ϕ	$[-]$
$\mathbf{s_u}$	User defined momentum source term	$[-]$
$\mathbf{S}$	Strain rate tensor	$[-]$
$\mathbf{T_{RANS}}$	Reynolds stress tensor	$[-]$
$\mathbf{T}$	Viscous stress tensor	$[-]$
$\mathbf{v}$	Velocity vector	$[m/s]$
$\mathbf{v}_g$	Grid velocity	$[-]$
$\overline{\mathbf{T}}$	Viscous stress tensor, time averaged	$[-]$
$\overline{\mathbf{v}}$	Velocity vector, time averaged	$[-]$
a_f	Face area	$[m^2]$
b	Specific body forces	$[-]$
d_s	Interaction length scale	$[-]$
E	Energy	$[J]$
f_b	Momentum source due to external body forces	$[-]$
f_i	User defined momentum source term for phase i	$[-]$
G	Grid flux	[-]
g	Gravitational acceleration	$[-]$
K	Consistency factor	$[-]$
k	Turbulent kinetic energy	$[-]$
m	Mass	$[kg]$
n	Power law exponent	$[-]$
p	Pressure	$[Pa]$
P_k	Turbulent kinetic energy production	$[-]$
Re_{ps}	Phase pair reynolds number for phases p nad s	$[-]$
S	Source term	[-]
S_ϕ	General source term	$[-]$
S_ε	Turbulent dissipation rate source term	$[-]$
S_k	Turbulent kinetic energy source term	$[-]$
S_u	User defined mass source term	$[-]$
t	time	$[s]$
T_e	Specific time scale	$[-]$
T_e	Turbulent time scale	$[-]$
u	x-velocity component	$[m/s]$

u', v', w'	Fluctuating velocity components	$[m/s]$
u^+	Dimensionless velocity	$[-]$
u_τ	Friction velocity	$[-]$
V	Cell Volume	$[m^3]$
v	y-velocity component	$[m/s]$
$v_{d,i}$	Drift velocity for phase i	$[m/s]$
v_{ps}	Phase relative velocity	$[m/s]$
w	z-velocity component	$[m/s]$
y	Closest distance to a wall	$[m]$
y^+	Dimensionless wall distance	$[-]$
Y_i	Mass fraction for phase i	$[-]$
α	Shear coefficient	[-]
α_i	Volume fraction of phase i	$[-]$
$\dot{\gamma}$	Strain rate	$[-]$
Γ	Diffusive flux tensor	$[-]$
μ	Dynamic viscosity	$[kg/m^2s]$
μ_0	Threshold viscosity at yield stress	$[-]$
μ_t	Turbulent viscosity	$[kg/m^2s]$
ν	Kinematic viscosity	$[m^2/s]$
$\overline{\phi}$	General variable, time averaged	$[-]$
ϕ	General variable, instantaneous	$[-]$
ϕ'	General variable, fluctuating component	$[-]$
ρ	Density	$[kg/m^3]$
σ	Overall stress tensor	$[-]$
τ_0	Yield stress	$[-]$
τ_w	Wall shear stress	$[-]$
ε	Turbulent dissipation rate	$[m^2/s^3]$
ε	Turbulent kinetic energy dissipation	$[-]$
ε_0	Ambient value of turbulent dissipation rate	$[-]$
P_ε	Turbulent dissipation rate production	$[-]$
τ_{sps}	Phase pair relaxation time	$[-]$

Coefficients

C_μ,$C_{\varepsilon 1}$,$C_{\varepsilon 2}$,σ_ε,σ_k	Realizable $k-\epsilon$ turbulence model coefficients
C_D	Schiller-Naumann drag coefficient
f_μ,f_2	Damping coefficients
f^{ps}_{drag}	Phase pair drag coefficient

Subscripts

0	Current cell index
d	diffusion
f	Face
i	Phase index

i, j, k	Newtons indices
n	Arbitrary cell index
p	Primary phase
ps	Phase pair
s	Secondary phase

Abbreviations

BDF	Backward Differentiation Formula
CFD	Computational Fluid Dynamics
DNS	Direct Numerical Simulation
MRF	Moving Reference Frame
RANS	Reynolds Averaged Naiver Stokes
TKE	Turbulent Kinetic Energy
TS	Total Solids
VOF	Volume of Fluid
WWTP	Waste Water Treatment Plant

Contents

List of Figures

List of Tables

1 Introduction

This section provides a background of the operation and underlying mechanical principle of a typical decanter centrifuge and its application in municipal sewage treatment, which is the focus of this study. The purpose and objectives of the study are also briefly discussed.

1.1 Decanter centrifuge

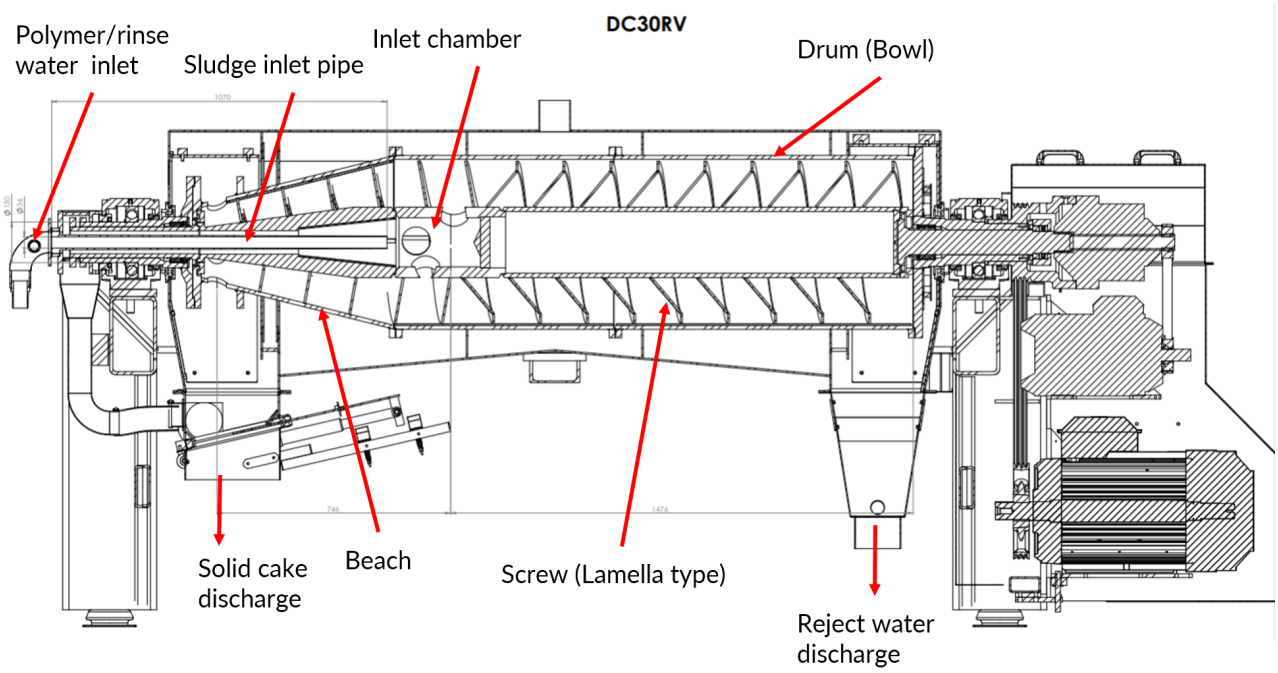

Figure 1.1: *Layout of a counter-current horizontal decanter centrifuge*

The solid-bowl scroll-discharge centrifuge, more commonly known as the decanter centrifuge is a device that is used to separate solid substances suspended in liquids, utilizing the density difference between the two phases. The most basic decanter centrifuge consists mainly of a cylindrical drum

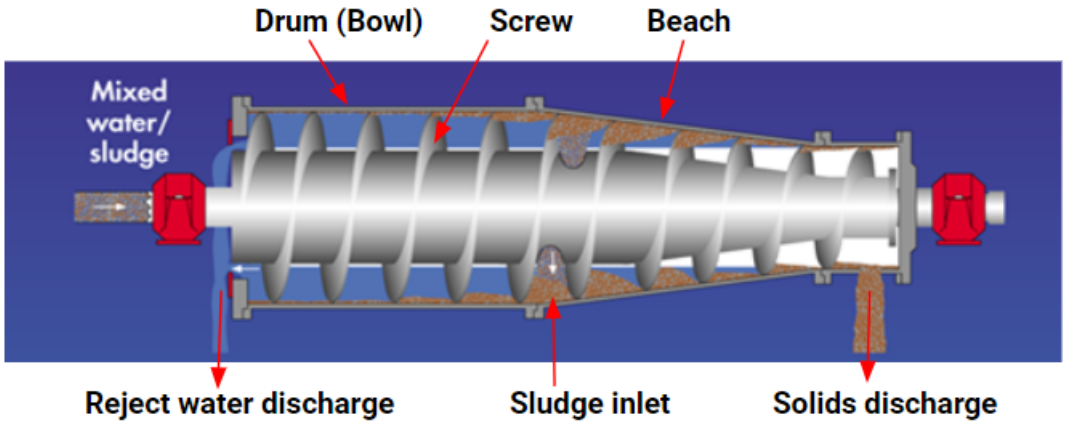

Figure 1.2: *Simplified schematic of a decanter centrifuge (counter-current type)*

also know as the bowl with an Archimedes' screw mounted within the drum. One end of the drum and the screw tapers towards the axis of the drum. The mixture to be separated is pumped into a feed zone present inside the screw. The slurry then enters the space between the screw and the drum through holes present in the feed zone. The drum and the screw inside it are rotated at a high speed exerting a huge centrifugal force on this slurry. The difference in density between the liquid and the solid particles suspended within the liquid exerts unequal amounts of centrifugal force on these phases. The heavier phase settle towards the wall of the drum whereas the lighter phase floats on top of it. The screw is rotating at a speed which is a few rpm slower than the drum. If viewed from the reference frame of the drum, the screw would appear to be rotating within a stationary drum at the differential speed, in the opposite direction. This rotating screw conveys the solid particles towards and up the tapered end of the drum where they are discharged in the form of a sludge cake which is relatively drier than the slurry that was fed into the centrifuge. The clarified liquid flows along the bowl and is discharged out at the other end[2]. There are dozens of variants of decanter centrifuges available in the market today that differ in terms of the design of the feed zone, screw, drum, polymer mixing mechanism etc. The description provided here is based on one of the centrifuges manufactured by a Swedish company, Noxon. CFD simulation of the flow within such a decanter centrifuge is the focus of this project.

1.2 Slurry

1.2.1 Dewatering

Although a decanter centrifuge has a wide range of industrial applications, one of its most important uses is in 'dewatering'. During the final stages of the treatment of domestic sewage slurry at Waste Water Treatment Plants (WWTP), there is a large amount of water present in the slurry along with solid residue left behind after the treatment process. This slurry cannot be directly dumped due to environmental concerns. The solids present in the slurry are great natural agricultural fertilizers and can also be used in filling up landfills. The water can be treated further and then dumped safely into a water body. This process of separation of these two phases from the slurry is known as dewatering [4].

A decanter centrifuge is one of the machines used to accomplish this separation. Under the action of centrifugal forces generated within the decanter, the heavier solid phase sediments out of the lighter liquid phase. The solid particles suspended in the slurry also contain absorbed water, which under the action of the centrifugal force is squeezed out of these particles. As the solids are conveyed up the beach (conical end) by the screw, they get compacted and even more water is squeezed out. The result is a relatively dry paste like cake obtained at the solids discharge outlet known as the sludge cake and almost clean water at the water discharge outlet known as the reject water. The water is not completely clean as it still contains certain dissolved solids and superfine particles which could not be sedimented out and hence needs further treatment to remove these.

1.2.2 Flocculation

The dewatering of such slurries is greatly influenced by their mechanical properties, most notably by the size of the solid particles present within the slurry. Smaller particles being lighter, are difficult to sediment out as compared to larger, heavier particles[2]. In addition to this, a larger number of small particles as opposed to fewer large particles means a higher surface area to volume ratio, which contributes to resistance against dewatering due to complex physical and chemical phenomena. Slurries with larger particle sizes are thus beneficial for dewatering performance[5]. Particle sizes in the slurry are increased through a process known as chemical conditioning wherein certain flocculating chemicals are mixed into the slurry before or during the dewatering process. These chemicals encourage

smaller particles to be agglomerated into aggregates known as flocs either through coagulation or by trapping them within other larger floc networks. Poly-electrolytes have become the flocculating agent of choice especially when it comes to dewatering of municipal sewage slurries using centrifuges. These poly-elctrolytes are water soluble polymers whose role is essentially to destabilize sub-colloidal particles (particles with size $< 10\mu m$) and bind them into larger flocs[4]. The use of such polymers has become ubiquitous to improve the dewaterability of such slurries using decanter centrifuges[6].

1.2.3 Slurry rheology

Rheology of the slurry is also an important parameter that governs how the slurry would flow (strain) under the application of a force (stress). It can also be defined as the viscous characteristics of the slurry. The treated sewage slurry to be dewatered through decanter centrifuges is known to show non-newtonian behaviour meaning that the strain rate produced in the fluid is not linearly proportional to the shear stresses applied to it[7]. The non-newtonian behavior becomes more pronounced at higher solid concentrations[8]. This also means that knowing the rheology at the inlet to the decanter is not enough, as the solid concentration within the centrifuge and thus the overall rheology of the fluid varies greatly from point to point. The rheology is also greatly influenced by the polymer dosage [9]. In addition to these factors, the rheology of the slurry itself varies from place to place depending on its biological and chemical composition, season of the year, and treatment steps it has undergone prior to dewatering. The slurry has also been found to be thixotropic meaning that its rheology changes with time due to aging and microbial activity[10].

In summary, defining a material model for the slurry is not a straightforward task due to large variations in its rheological characteristics, influence of local solids concentration, biological activity etc. This means that experimental data taken from measurement of physical parameters are often unreliable and a standard reference material cannot be defined based on such data. Suitable simplifications are needed to be made where possible to obtain an approximate general definition of the material properties that represents a wide range of sewage slurries that could be encountered in a typical dewatering operation. These simplifications have been detailed in sec.(3.3).

1.3 Purpose of the study

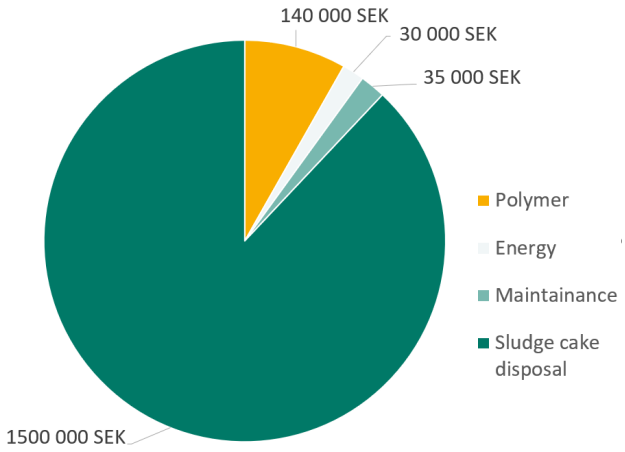

(a) *Operating costs in SEK*

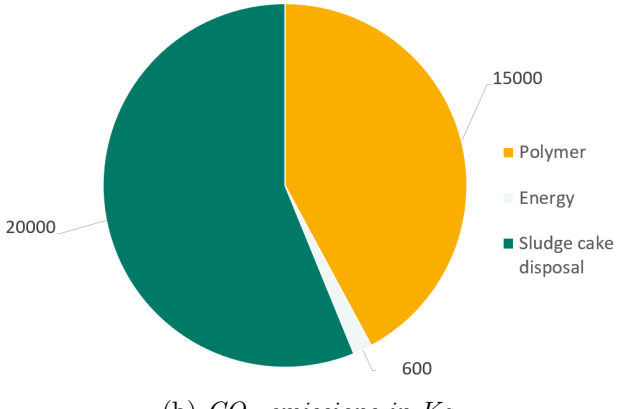

(b) *CO_2 emissions in Kg*

Figure 1.3: *Annual operating costs and CO_2 emissions associated with a typical municipal sewage sludge dewatering operation at a WWTP somewhere in Sweden (Noxon AB)*

The impetus behind studying the dewatering process within a decanter centrifuge is mainly based on environmental and economic factors. The sludge cake obtained after the dewatering process is used as an agricultural fertilizer and hence needs to be transported from WWTPs to farmlands which is accomplished mainly through trucks. A drier, hence lighter sludge cake means reduced transport costs which is the major cost in this whole operation[4]. Additionally, better dewaterabilty using lower amounts of polymer helps combat water pollution as the amount of biosolids and the flocculating polymer being dumped into water bodies is reduced[2]. Figure.(1.3) reiterates just how substantial the costs associated with the disposal of the dewatered sludge cake are. Obtaining a drier sludge cake is thus paramount in reducing these costs and making the operations more sustainable.

The goal of this project is to contribute in developing a working computational model that can be used as a tool to study the influence of various operational and design parameters on the dewatering performance of a decanter centrifuge. The data on how a particular parameter influences the flow and the dewatering performance can be valuable when designing a new machine. A reliable computational model would cut down the number of experimental studies needed to be done in order to obtain relevant data, hence drastically lowering the research and development costs. It can also provide insights into phenomena that cannot be studied through purely experimental models. The objective of the study is thus the development of a methodology to resolve the flow inside a decanter centrifuge separating municipal sewage sludge. Upon obtaining such a model, comparisons can be made by varying different parameters such as the slurry rheology, mass flow rate of the slurry, etc.

2 Theory

This section provides a description of what CFD is and the various aspects of fluid flow that are relevant in this project. The corresponding equations have also been discussed to provide a better understanding of what the CFD solver is actually doing.

2.1 Computational fluid dynamics

Computational fluid dynamics generally involves representing any physical fluid flow system being analysed as a mathematical model consisting of a system of partial differential equations which govern the flow physics within the system. Solving these equations yields the distribution of relevant flow variables such as velocity, pressure, temperature etc., within the computational domain. Solving this set of differential equations requires that suitable boundary and initial values for the relevant variables are applied. Appropriate specification of initial and boundary conditions also depends on the physical nature of the differential equations involved which can be elliptical, parabolic, hyperbolic, or a combination of these[11]. Practical fluid flow cases are therefore almost impossible to generalise and solve due to their complex and diverse nature. In most CFD codes, these equations are instead transformed into integrals that represent the exact conservation of the relevant variables within a finite sized element. The computational domain is then divided into a finite number of these elements. For time marching or unsteady problems, a similar division is made in time wherein the total time needed to be simulated is subdivided into a number of time-steps. This division carried out in space and time is known as discretization and it transforms the set of differential equations into a set of algebraic equations which can then be solved for in each element using numerical methods[12]. This is known as the finite-volume method. Although algebraic equations make it tractable to generalise CFD codes, they require iterative solution methods due to the complex and non-linear nature of the underlying physical phenomena. These numerical solution procedures do not result in the exact solution, but asymptote to the solution to the set of equations. The degree of accuracy of the obtained solution depends on factors such as the users ability to formulate the mathematical model, numerical schemes used, discretization of the domain in space and time etc. which further depend on the availability of computational resources, time, and the degree of accuracy desired by the user.

2.1.1 General transport equation

$$\underbrace{\frac{d}{dt}\int_V \rho\phi dV}_{\text{Transient term}} + \underbrace{\oint_A \rho\mathbf{v}\phi\cdot d\mathbf{a}}_{\text{Convective flux}} = \underbrace{\oint_A \Gamma\nabla\phi d\mathbf{a}}_{\text{Diffusive flux}} + \underbrace{\int_V S_\phi dV}_{\text{Source term}} \tag{2.1}$$

The four terms in eqn. (2.1) signify the following:

1. Transient term: Rate of change of the variable ϕ within the control volume, with respect to time.
2. Convective flux: Net rate of decrease of ϕ within the control volume due to its convection across the control volume boundaries.
3. Diffusive flux: Net rate of increase of ϕ within the control volume due to its diffusion across the control volume boundaries.
4. Source term: Net rate of addition of ϕ to the control volume due to some sources present within the control volume.

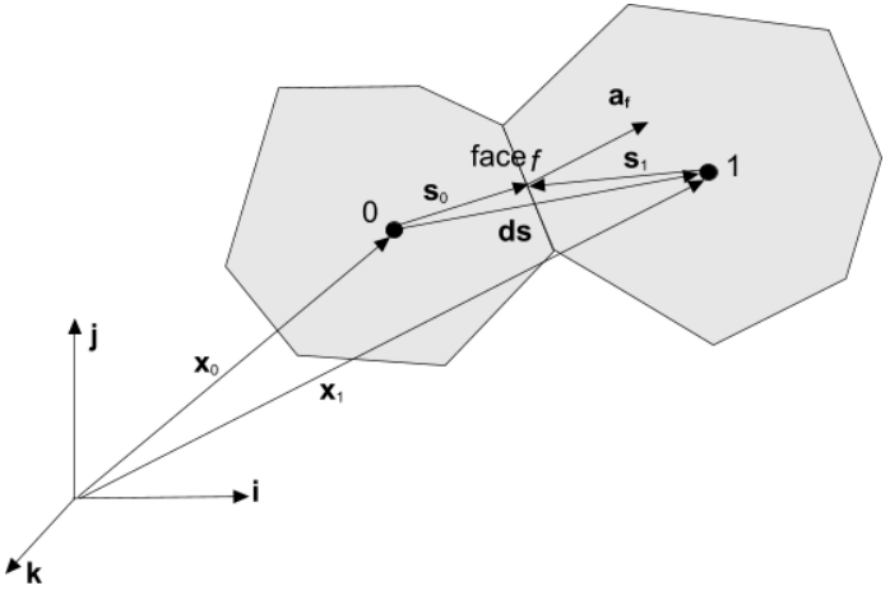

Figure 2.1: *Finite volume discretization in space using polyhedral cells[1]*

Equation (2.1) represents the general transport equation in its integral form for a generic flow variable ϕ over a finite control volume V. Here ϕ is a general scalar variable that is being transported through the fluid. It can be replaced with an appropriate quantity to obtain the transport equation for relevant flow variables. For example replacing it with 1, u, v, w, or E yields the conservation equations for mass, momentum (in i, j, and k directions), or energy respectively for a finite-volume element.

The cell values of volume and surface integrals in eqn.(2.1) need to be approximated by the solver. The volume integral of the source term for example, is approximated as $\int_V S_\phi dV \approx S_{\phi_0} V_0$. This assumes that the source term has a constant value S_0 within a cell with volume V_0. S_0 is approximated to the mean value of S_ϕ within the cell. The surface integral is approximated as $\oint_A \mathbf{J}^\phi \cdot d\mathbf{a} \approx \Sigma_f \mathbf{J}^\phi \cdot \mathbf{a}_f$. Here, J^ϕ is the flux of any property ϕ through face f. The flux at each face is taken to be the product of the value of flux at the face center and face area $\mathbf{a}_f$. The flux at face centers are evaluated through interpolation of respective cell center values. This transforms the equation into its semi-discretized form shown in eqn. (2.2). The equation is discretized in space but is yet to be discretized in time.

$$\frac{d}{dt}(\rho\phi V)_0 + \Sigma_f[\rho\phi(\mathbf{v}\cdot\mathbf{a})]_f = \Sigma_f[\Gamma\nabla\phi\cdot\mathbf{a}]_f + (S_\phi V)_0 \tag{2.2}$$

The temporal term is discretized using a second order discretsation scheme known as the Backward Differentiation Formula (BDF). BDF2 is shown in eqn.(2.3). The '2' indicates that the solution from two previous timesteps have been used to approximate the transient term. Higher levels of the BDF can be obtained through a linear combination of BDFs.

$$\frac{d}{dt}(\rho\phi V)_0 = \left(\frac{3}{2}(\rho\phi V)_{n+1} - 2(\rho\phi V)_n + \frac{1}{2}(\rho\phi V)_{n-1}\right)\frac{1}{\Delta t} \tag{2.3}$$

2.1.2 Mass and Momentum

The fundamental equations of conservation of mass, momentum, and energy applied to any fluid flow co-relate the velocity, pressure, density, and temperature distribution within the fluid. These

equations also known as the Navier-Stokes equations are a set of coupled partial differential equations that are too complex to be solved analytically through calculus for most fluid flows of practical importance. Although as explained in the beginning of this chapter, these equations can be converted into integrals over finite control-volumes and solved using numerical techniques. The conservation equation for mass (continuity equation) and momentum integrated over a control volume V are shown in eqns.(2.4) and (2.5).

$$\frac{\partial}{\partial t}\int_V \rho dV + \oint_A \rho \mathbf{v} \cdot d\mathbf{a} = \int_V S_u dV \tag{2.4}$$

$$\frac{\partial}{\partial t}\int_V \rho \mathbf{v} dV + \oint_A \rho \mathbf{v} \otimes \mathbf{v} \cdot d\mathbf{a} = -\oint_A p\mathbf{I} \cdot d\mathbf{a} + \oint_A \mathbf{T} \cdot d\mathbf{a} + \int_V \mathbf{f_b} dV + \int_V \mathbf{s_u} dV \tag{2.5}$$

The terms S_u and $\mathbf{s_u}$ denote user defined mass and momentum source terms respectively. The term f_b is also a kind of a momentum source term, that comes into play due to external body forces such as gravitational, centrifugal, Coriolis, and electromagnetic forces. Comparing eqn.(2.5) with eqn.(2.1), notice that the diffusive flux term has been split into two terms. The first term on the right hand side corresponds to the diffusion due to normal stresses induced by pressure p and the second term corresponds to the diffusion of momentum due to viscous shear stresses, where $\mathbf{T}$ is the viscous stress tensor. For a newtonian fluid, $\mathbf{T}$ is defined as $\mathbf{T} = 2\mu\mathbf{S} - \frac{2}{3}\mu(\nabla \cdot \mathbf{v})\mathbf{I}$ where, $\mathbf{S} = \frac{1}{2}(\nabla\mathbf{v} + (\nabla\mathbf{v})^T)$ is the strain rate tensor.

It can be clearly seen in eqn.(2.5) that the pressure field is required to solve the momentum equation. This pressure field needs needs to be obtained somehow while making sure that the velocity field obtained using the momentum equation also satisfies continuity. One way to ensure this is to obtain a direct solution to the set of equations (2.4) and (2.5). Such a solution is not possible as discussed earlier and is the reason behind the use iterative solution methods. Doing so results in a special type of numerical error known as checker-boarding wherein unrealistic highly oscillating pressure fields may arise during the iterative solution procedure. This is not the main issue as the iterative solution should eventually converge to the correct pressure field. Although due to the way in which finite volume discretization works, this oscillating pressure field is felt by the momentum equation through a zero pressure gradient term or in other words as a uniform pressure field. Since there is no pressure gradient, the velocity fields would not be updated, thus preserving the unrealistic pressure field until convergence leading to a highly absurd solution. In order to avoid this, a procedure known as the SIMPLE algorithm was developed by Patankar and Spalding (1972). The details of this algorithm are not discussed here for conciseness but can be found in [12]. In this study, the solver, Star-CCM+ utilizes the SIMPLE algorithm for the coupling of pressure and velocity fields.

2.1.3 Mesh Motion

Many cases of fluid flow calculations involve motion of some part or even the entire domain with respect to an absolute reference frame. Modelling such a motion is in essence a time-marching problem. This means that that the evolution of the fluid flow with time needs to be resolved while simultaneously modifying the orientation of the entire or atleast some part of the domain according to the desired motion. This would involve creating a new mesh after every time-step and hence make the calculations enormously expensive. Numerous methods have been developed in order to simplify the analysis of such problems that mainly involve avoiding the creation of a new mesh or even doing away with the transient nature of the problem.

One such technique is the sliding mesh approach. In this approach, the mesh within the domain or a certain region in the domain is treated as a rigid body. The motion is then applied to this region by actually moving it as required. An interface needs to be created between the static and the moving regions of the mesh if such a demarcation exists. The moving region thus 'slides' in contact with the static region. The sliding mesh approach does not require a new mesh to be created at every timestep. This approach can readily be applied to simple motions such as rotation or oscillatory motion.

$$\frac{\partial}{\partial t}\int_V \rho dV + \oint_A \rho(\mathbf{v}-\mathbf{v_g})\cdot d\mathbf{a} = \int_V S_u dV \tag{2.6}$$

$$\frac{\partial}{\partial t}\int_V \rho\mathbf{v} dV + \oint_A \rho\mathbf{v}\otimes(\mathbf{v}-\mathbf{v_g})\cdot d\mathbf{a} = \oint_A \sigma\cdot d\mathbf{a} + \int_V \mathbf{f_b} dV + \int_V \mathbf{s_u} dV \tag{2.7}$$

Due to motion of the mesh itself, the convective terms in eqn.(2.6), and (2.7) contain additional contributions due to the mesh velocity (also known as the grid velocity), $\mathbf{v_g}$. In the discretized form of the general transport equation (eqn.(2.2)), the convective term is modified by defining an additional flux term due to the mesh motion. The convective term in eqn.(2.2) thus becomes $[\rho\phi(\mathbf{v}\cdot\mathbf{a}-G)]_f = \dot{m}_f\phi_f$. Where G is the additional flux contribution known as grid flux. The exact definition of the diffusive, convective, and grid flux terms are given by eqns.(A.1), (A.3), and (A.4) respectively in appendix.

Sliding mesh is one of the most accurate approaches to model mesh motion, second only to a completely dynamic mesh which updates the whole mesh at every time-step. But it is still a transient approach and hence requires appropriately fine discretization in time and hence can prove to be quite computationally demanding. In a limited number of cases, the problem can be solved using a steady state approach known as the Moving Reference Frame(MRF) approach. In MRF, the mesh does not move at all. But the zone in which the motion is to be applied is considered to be in a separate frame of reference. This non-inertial reference frame is defined with respect to a stationary, or an absolute reference frame. The motion of the non-inertial reference frame gives rise to inertial forces that act on the entire fluid volume in that zone. These forces need to be accounted for while performing the calculations. In most cases these forces are not negligible and are actually responsible for the fluid flow to occur in the first place. The most common example of such a force is the centrifugal force exerted due to the rotation of an impeller in a centrifugal blower or pump. It must be noted that there are certain severe restrictions when it comes to using the MRF approach such as the axis-symmetry of the geometry, the proximity of any surrounding solid surfaces that are not a part of the MRF etc.

2.1.4 Turbulence modelling

Most practical fluid flow cases encountered are turbulent in nature. Turbulent flow mainly consists of fluctuating eddies with a variying range of sizes. In order to completely resolve a turbulent flow flow field, each and every turbulent eddy within the flow needs to be resolved. Some of these eddies have minute length and time scales when compared to the corresponding flow scales. This requires a very fine computational grid and a very short time-step. The computations for practical applications thus become extremely expensive. One of the ways to circumvent this problem, is to decompose the instantaneous field variables such as velocity, temperature, pressure etc. into its mean and fluctuating value. A general variable ϕ is decomposed into its mean value $\overline{\phi}$ and instantaneous fluctuating value ϕ' in eqn.(2.8).

$$\phi = \overline{\phi} + \phi' \tag{2.8}$$

Decomposing the velocity into its mean and fluctuating component and inserting it into the Navier-stokes equations (eqns.(2.4), and (2.5)) followed by some mathematical simplifications, we obtain the

conservation equations for mass (eqn.(2.9)) and mean momentum (eqn.(2.10)) of a turbulent flow. These equations are known as the Reynolds Averaged Navier-Stokes (RANS) equations.

$$\frac{\partial}{\partial t}\int_V \rho dV + \oint_A \rho\overline{\mathbf{v}}\cdot d\mathbf{a} = \int_V S_u dV \tag{2.9}$$

$$\frac{\partial}{\partial t}\int_V \rho\overline{\mathbf{v}} dV + \oint_A \rho\overline{\mathbf{v}}\otimes\overline{\mathbf{v}}\cdot d\mathbf{a} = -\oint_A \overline{p}\mathbf{I}\cdot d\mathbf{a} + \oint_A (\overline{\mathbf{T}} + \mathbf{T_{RANS}})\cdot d\mathbf{a} + \int_V \mathbf{f_b} dV + \int_V \mathbf{s_u} dV \tag{2.10}$$

Similar to the Navier-Stokes equations, the RANS equations are essentially the conservation equations for mass and mean values of momentum respectively. The new term $\mathbf{T_{RANS}}$ in eqn.(2.10), comes into picture due to the fluctuating component of the velocity. It constitutes an additional stress due to the fluctuating velocities and is known as the Reynolds Stress tensor.

$$\mathbf{T_{RANS}} = -\rho\begin{pmatrix}\overline{u'u'} & \overline{u'v'} & \overline{u'w'}\\ \overline{v'u'} & \overline{v'v'} & \overline{v'w'}\\ \overline{w'u'} & \overline{w'v'} & \overline{w'w'}\end{pmatrix} + \frac{2}{3}\rho k\mathbf{I} \tag{2.11}$$

Where $k = \frac{1}{2}(\overline{u'u' + v'v' + w'w'})$ is the turbulent kinetic energy. $\mathbf{T_{RANS}}$ is unknown as it contains all the unknown fluctuating components. Thus it needs to be modelled to provide a closure for the RANS equations.

Boussinesq approximation

Closure to the system of RANS equations can be achieved through modelling them in terms of the mean flow quantities, most commonly through an assumption known as the boussinesq approximation[13] which introduces a turbulent/eddy viscosity μ_t to model the unknown Reynolds Stress tensor.

$$\mathbf{T_{RANS}} = 2\mu_t\mathbf{S} - \frac{2}{3}(\mu_t\nabla\cdot\overline{\mathbf{v}})\mathbf{I} \tag{2.12}$$

Where $\mathbf{S} = \frac{1}{2}(\nabla\overline{\mathbf{v}} + \nabla\overline{\mathbf{v}}^T)$ is known as the strain rate tensor. It has a magnitude $S = |\mathbf{S}| = \sqrt{2\mathbf{S}:\mathbf{S}^T}$. The problem of finding the unknown fluctuating components is now replaced with determining the turbulent viscosity μ_t which varies throughout the flow field.

The $k-\epsilon$ model

One of the ways in which this can be done is by solving the transport equation for the turbulent kinetic energy k (eqn.(2.13)) and the turbulent dissipation rate ϵ (eqn(2.14)).

$$\frac{\partial\rho k}{\partial t} + \nabla\cdot(\rho k\overline{\mathbf{v}}) = \nabla\cdot\left[\left(\mu + \frac{\mu_t}{\sigma_k}\right)\nabla k\right] + P_k - \rho(\varepsilon - \varepsilon_0) + S_k \tag{2.13}$$

$$\frac{\partial\rho\varepsilon}{\partial t} + \nabla\cdot(\rho\varepsilon\overline{\mathbf{v}}) = \nabla\cdot\left[\left(\mu + \frac{\mu_t}{\sigma_\varepsilon}\right)\nabla\varepsilon\right] + \frac{1}{T_e}C_{\varepsilon 1}P_\varepsilon - C_{\varepsilon 2}f_2\rho\left(\frac{\varepsilon}{T_e} - \frac{\varepsilon_0}{T_0}\right) + S_\varepsilon \tag{2.14}$$

The turbulent viscosity is computed using the relation $\mu_t = \rho C_\mu f_\mu \frac{k^2}{\varepsilon}$.
Where,

- $T_e = \dfrac{k}{\varepsilon}$: is the turbulent time-scale.
- $T_0 = max\left(\dfrac{k_0}{\varepsilon_0}, C_t\sqrt{\dfrac{\nu}{\varepsilon_0}}\right)$: is the specific time-scale. The subscript '0' indicates the ambient values of the turbulence variables, or in other words the values in the vicinity of a wall surface[14]. This term is used as a source term to counteract the effects of turbulence decay[1].
- $P_k = f_c\left(\mu_t S^2 - \dfrac{2}{3}\rho k\nabla\cdot\overline{\mathbf{v}} - \dfrac{2}{3}\mu_t(\nabla\cdot\overline{\mathbf{v}})^2\right)$: is the production term in the transport equation for turbulent kinetic energy. It corresponds to the production of turbulent kinetic energy by large length-scale eddies that interact with the mean flow and extract energy from it.
- $P_\varepsilon = f_c S k$: is the production term in the transport equation for turbulent dissipation. It does not have much of a physical significance but is more of a consequence of the way in which the this equation is derived.
- σ_k, σ_ϵ, $C_{\varepsilon 1}$, $C_{\varepsilon 2}$, f_c, f_μ, f_2, C_μ, and C_t are model coefficients and are detailed in the appendix(A.4). S_k and S_ϵ are user defined source terms.

The model described above is the Realizable $k-\varepsilon$ model detailed in [15]. This approach of modelling the Reynolds Stress tensor falls under the broad category of Eddy Viscosity models. It is one of the most common models used currently for industrial flows, due to its versatility and computational efficiency.

Wall modelling in turbulent flow

Turbulent flow close to walls is not as straight forward as one might think and requires some special attention. It is convenient to non-dimensionalize parameters such as the wall distance and velocity to make comparison among flows easier. This is usually done through scaling these variables with quantities related to the wall. A wall friction velocity can be defined based on the shear stress at the wall τ_w as $u_\tau = \left(\dfrac{\tau_w}{\rho}\right)^{1/2}$. This quantity is then used to scale the wall distance as $y^+ = \dfrac{yu_\tau}{\nu}$ with y being the closest physical distance to any wall.

Figure (2.2) shows the scaled velocity profile plotted against the scaled wall distance, taken from high accuracy DNS simulations [16]. Turbulent boundary layer close to walls can be divided into an inner layer and an outer layer. The figure shows mainly the inner layer ($y^+ < 300$ in this case but this limit increases with increasing flow Reynolds's number[13]). The inner layer can further be subdivided into three zones, each having unique flow characteristics and behaviour. The inner most layer, adjacent to the wall is the viscous sub-layer. The flow here is dominated by viscous effects and is almost laminar. $u^+ = y^+$ in the viscous sub-layer. The outermost zone in the inner layer is the log-law zone, also known as the inertial sub-layer. This region is dominated by turbulent diffusion, and the scaled velocity varies logarithmically with the wall distance as $u^+ = ln(y^+)/0.41 + 5.2$. The viscous effects in this zone are almost negligible. The buffer layer in the middle is just a transition between these two zones.

The interaction of turbulent flows with walls is complex. Flow moving relative to walls is a source of vorticity leading to an overall increase in the turbulence intensity of the flow, also altering the boundary layer profiles for various flow quantities. This leads to sharp gradients in the boundary layer that become steeper with increasing flow Reynold's number. Thus a fine mesh is required close to the

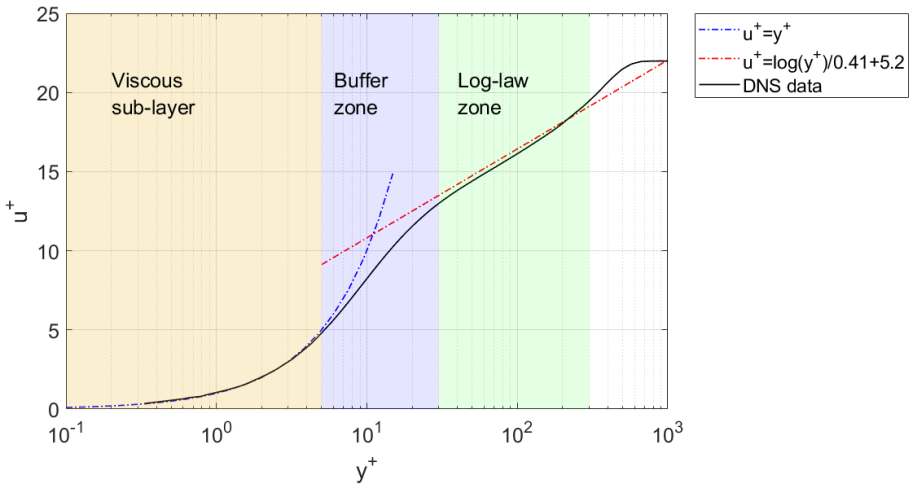

Figure 2.2: *Non-dimensional velocity profile of flow along a flat plate showing the turbulent boundary layer (DNS data taken from Spalart and Philippe (1988))*

walls in order to resolve such gradients, making the computations expensive. Models are required to mitigate this problem, and resolve the effects of the presence of the wall without using a super-fine mesh.

The model used by the solver in this project is the Two-layer approach. In this approach, the turbulent dissipation rate ε and turbulent visocity μ_t are set to prescribed values proportional to the wall distance within the viscous sub-layer. These values are then blended with their computed values away from the near wall region. This model allows the use of relatively coarser meshes close to the walls [1].

2.1.5 Multiphase modelling

Multiphase flows cover a wide array of fluid flow problems involving two or more immiscible phases. These phases being solids, liquids, or gasses. This makes developing generalized governing equations for such problems extremely difficult.

Many multiphase flows are resolved through a lagrangian approach where all or some of the phases are no longer treated as continua but as a collection individual particles. The particles can be solid particles, liquid droplets, or gas bubbles, or a parcel consisting of a finite number of any of these three entities. A phase is then modelled with a finite number of these particles that can interact with each other, with other phases that my be modelled as a continua, as well as boundaries of the domain. Equations based on newtons laws of motion are solved for each of these particles to study the evolution of the flow in time. Although such an approach is better suited for realtively dilute flows where the number of particles can be kept relatively low. In an application such as the decanter centrifuge, the number of particles required to model the flow would be enormous and would hence increase the computational cost dramatically.

In principle, a multiphase flow could be represented with the whole flow field consisting of a single continua, wherein each separate phase is represented by its boundaries with the neighbouring or in many cases a surrounding phase. The boundaries decide where one phase ends and the other phase begins. This is the basis of Eulerian Multiphase modelling. Although in practice this approach is not that straightforward due to the fact that the thickness of the interface-boundary is infinitesimally small, whereas the cells of the numerical grid are of a finite size. The interfacial-boundaries are a part of the solution and so a reasonably accurate solution requires a super-fine computational mesh

in eulerian interface modelling approaches such as the Volume of Fluid (VOF) approach and we run into numerical problems when using semi-lagrangian methods such as front-tracking or level-set[17] which means these approaches would be expensive and unreliable in the absence of relevant data.

A simpler multiphase-modelling approach is to treat the phases as interpenetrating continua with each phase having a variable associated to it known as the volume fraction. The volume fraction of a phase at a point is always between 0 and 1. 0 meaning that the phase is completely absent at that location and 1 meaning only that phase is present at that location. Appropriate models are required to faithfully simulate the interfacial transfer of mass, momentum and energy. These models differ based on the combination of phases present in the flow (gas-solid, solid-liquid, liquid-liquid etc.) and also on the nature and geometry of the interface between these phases (continuous or dispersed)[18].The most general approach based on the interpenetrating-continua assumption works by treating each phase as a fluid entity and solves the transport equations for mass, momentum and energy transport for each phase. These transport equations further contain source-terms to model the interfacial interactions but the definition of such source terms is more often than not quite complicated, and unavailable. Improper specification of these interactions, especially in the momentum equations is common and often leads to numerical instabilities[19]. This approach is known commonly as the Segregated Eulerian approach as we are segregating the variable transport equation for each phase.

The Mixture Multiphase Model

These problems can, to a great extent be alleviated by formulating the transport equations in terms of the mixture of phases. Although this does not necessarily mean that the component phases also move with the same velocity as the mixture. In the presence of strong body forces such as gravitational or centrifugal forces, individual phases can move relative to the volume center of the mixture. These velocity differences are accounted for based on assumptions of local equilibrium. A drift/slip velocity is used to express the relative motion of each phase with respect to the volume center of the mixture. The set of constitutive kinematic relations for the drift flux has been developed and validated by Ishii[20]. This approach is known as the mixture multiphase model and it simplifies the problem significantly as compared to solving for each phase separately. The mixture model is more suitable for multi-phase flows where the coupling between the phases is strong. The simplicity of the mixture model along with the drift-flux formulation, and its applicability to a wide range of multiphase flows of practical importance has made it a model of considerable importance for engineering applications [18].

The mixture model solves a transport equation for mass, momentum and energy for the entire mixture and an additional equation for the transport of volume fraction. The fourth equation is required to obtain the distribution of each phase within the domain. The transport equations for mixture mass, mixture momentum and phase volume fraction, discretized over a finite control volume are shown in eqns.(2.15), (2.16), and (2.22) respectively.

$$\frac{\partial}{\partial t}\int_V \rho_m dV + \oint_A \rho_m \mathbf{v}_m \cdot d\mathbf{a} = \int_V S_u dV \tag{2.15}$$

$$\begin{aligned}\frac{\partial}{\partial t}\int_V \rho_m \mathbf{v}_m dV + \oint_A \rho_m \mathbf{v}_m \otimes \mathbf{v}_m \cdot d\mathbf{a} \\ = -\oint_A p\mathbf{I}\cdot d\mathbf{a} + \oint_A \mathbf{T}_m \cdot d\mathbf{a} + \int_V \mathbf{f_b} dV + \int_V \mathbf{s_u} dV - \Sigma_i \oint_A \alpha_i \rho_i \mathbf{v}_{d,i} \otimes \mathbf{v}_{d,i} \cdot d\mathbf{a}\end{aligned} \tag{2.16}$$

The mixture velocity, density, viscosity, and the drift velocity are defined in eqn.(2.17). The subscript 'i' indicates that a property corresponds to phase i, among the n phases being considered.

$$\mathbf{v}_m = \frac{1}{\rho_m}\Sigma_{i=1}^{n}\mathbf{v}_i\alpha_i\rho_i \qquad \rho_m = \Sigma_{i=1}^{n}\rho_i\alpha_i \qquad \mu_m = \Sigma_{i=1}^{n}\mu_i\alpha_i \qquad \mathbf{v}_{d,i} = \mathbf{v}_i - \mathbf{v}_m \tag{2.17}$$

$\mathbf{T}_m = \mu_m\Big[\big(\nabla\mathbf{v}_m + (\mathbf{v}_m)^T\big) - \frac{2}{3}(\nabla\cdot\mathbf{v}_m)\mathbf{I}\Big]$ is the viscous stress tensor with μ_m being the effective viscosity of the mixture calculated through volume weighted averaging of the dynamic viscosities of the constituent phase. The last term on the right hand of eqn.(2.16) corresponds to the momentum diffusion due to phase slip.

In order to compute the phase velocities, the drift velocity needs to be modelled. Consider the interaction between two phases being model. Let one of them be the primary phase denoted by the subscript p and the other be the secondary phase denoted by the subscript s. A relative velocity between the two phases is defined as $\mathbf{v}_{ps} = \mathbf{v}_s - \mathbf{v}_p$. This relative velocity is related to the drift velocity for primary phase through the relation, $\mathbf{v}_{d,p} = -\mathbf{v}_{ps} - \Sigma_i Y_i\mathbf{v}_{s,i}$, where $Y_i = \dfrac{\alpha_i\rho_i}{\rho_m}$ is the mass fraction of phase i.

The drift velocities for the primary and secondary phases can be calculated as:

$$\mathbf{v}_{d,p} = \frac{-v_0 - Y_s\mathbf{v}_{ps}}{Y_p + Y_s} \qquad \mathbf{v}_{d,s} = \frac{-v_0 + Y_p\mathbf{v}_{ps}}{Y_p + Y_s} \tag{2.18}$$

Where $v_0 = \Sigma_{i\notin\{p,s\}}Y_i\mathbf{v}_{d,i}$ is the contribution from drift velocities of all the other phases.

The relative velocity thus needs to be modelled and this is done in terms of a drag coefficient and a body force term as $\mathbf{v}_{p,s} = C_D\mathbf{b}$. Body forces are the reason behind differential phase velocities and hence it is only logical to formulate a model for the drift velocity based on them. The specific body forces $\mathbf{b}$ are defined as:

$$\mathbf{b} = \mathbf{g} - (\mathbf{v}_m\cdot\nabla)\mathbf{v}_m - \frac{\partial\mathbf{v}_m}{\partial t} \tag{2.19}$$

Where $\mathbf{g}$ is the acceleration due to gravity.

The drag coefficent C_D is provided by the Schiller-Naumann method. The Schiller-Naumann drag coefficient is computed by assuming that the primary phase is continuous and the secondary phase is dispersed. The drag coefficient is defined for the phase-pair interaction as:

$$C_D = C_D^{ps} = \frac{\tau_s}{f_{drag}^{ps}}\frac{\rho_s - \rho_m}{\rho_s} \tag{2.20}$$

$\tau_s = \dfrac{\rho_s d_s^2}{18\mu_p}$ is the particle relaxation time for the secondary phase. The drag coefficient is adjusted based on the phase pair Reynolds number Re_{ps} through the constant f_{drag}^{ps} as:

$$f_{drag}^{ps} = \begin{cases} 1 + 0.15Re_{ps}^{0.687} & \text{if } Re_{ps} \le 1000 \\ 0.0183Re_{ps} & \text{if } Re_{ps} > 1000 \end{cases} \qquad Re_{ps} = \frac{\rho_p|\mathbf{v}_{ps}|d_s}{\mu_p} \tag{2.21}$$

d_s is the interaction length-scale for the phase pair interaction and is a crucial parameter in adjusting the strength of coupling between phases.

Once the mixture velocity and drift velocity fields for all phases is obtained, the distribution of the phases in the domain is computed by solving a transport equation for the volume fraction shown in eqn.(2.22).

$$\frac{\partial}{\partial t}\int_V \alpha_i dV + \oint_A \alpha_i \mathbf{v}_m d\mathbf{a} = \int_V \left(S_{u,i} - \frac{\alpha_i}{\rho_i}\frac{D\rho_i}{Dt}\right)dV + \oint_A \frac{\mu_t}{\sigma_t \rho_m}\nabla\alpha_i \cdot d\mathbf{a} - \int_V \frac{1}{\rho}\nabla\cdot(\alpha_i\rho_i\mathbf{v}_{d,i}) \quad (2.22)$$

2.1.6 Rheology

Rheology describes the behaviour of a engineering materials under the action of some force (stress) and, seen in terms of the deformation (strain) under a set of loading and environmental conditions[21]. When dealing with fluids, this relationship between the applied stress and the induced strain is mainly described by the fluid viscosity. Fluids that show a linear relation between the stress and the strain (fluids with a constant viscosity, except for some gases where it can be dependent on the temperature) are termed as newtonian fluids and those that do not show a linear relationship (fluids whose viscosity is a function of the strain rate, temperature, and time among other things) are termed as non-netwonian fluids. Non-newtonian fluids is a very broad term consisting of a wide range of fluids that behave quite differently from each other.

For newtonian-fluids, the viscous stress tensor $\mathbf{T}$ is linearly related to the strain rate tensor $\mathbf{S}$ through a constant viscosity μ as:

$$\mathbf{T} = 2\mu\mathbf{S} - \frac{2}{3}\mu(\nabla\cdot\mathbf{v})\mathbf{I} \quad \text{where } \mathbf{S} = \frac{1}{2}(\nabla\mathbf{v} + (\nabla\mathbf{v})^T) \quad (2.23)$$

But many fluids do not exhibit this linear relationship. A Generalized newtonian fluid is the simplest mathematical description of a non-Newtonian fluid. In this case the viscosity is a function of the strain rate ($\dot{\gamma}$) and the temperature of the fluid. For a generalized newtonian fluid, the viscous stress tensor and the strain rate tensor are related through a strain rate dependent viscosity as:

$$\mathbf{T} = 2\mu(\dot{\gamma})\mathbf{S} \quad (2.24)$$

Note here that the second term in eqn.(2.23) has been omitted in eqn.(2.24) under the assumption of compressible flow which would make that term equal to zero due to continuity.

The simplest way to describe a strain rate dependent viscosity is through the power law $\mu(\dot{\gamma}) = K\dot{\gamma}^{n-1}$, where K is the consistency factor. The power law index, $n = 1$ corresponds to a newtonian fluid, $n > 1$ corresponds to a shear thickening fluid(viscosity increases with increasing shear), and $n < 1$ corresponds to a shear thinning fluid(viscosity decreases with increasing shear).

Another class of non-newtonian fluids are viscoplastic fluids. These fluids exhibit an initial resistance to yielding, known as the yield stress. If the stress applied is below the yield stress, there is negligible deformation and as the stress exceeds this limit, the material starts to flow. The viscosity of the fluid below the yield stress is infinitesimally high and drops to finite values as this stress limit is crossed. The relation between the visocus stress tensor and the strain rate tensor of a viscoplastic material, above the yield stress limit is described as:

$$\mathbf{T} = \mathbf{T}_0 + 2\mu(\dot{\gamma})\mathbf{S} \quad (2.25)$$

The Hershel-bulkley model is used to describe strain dependent viscosity in this case. It is a combination of a generalized newtonian fluid described using power law and a viscoplastic fluid.

$$\mu(\dot{\gamma}) = \begin{cases} \mu_0, & \text{if } \dot{\gamma} < \dfrac{\tau_0}{\mu_0} \\ \dfrac{\tau_0 + K\left(\dot{\gamma} - \dfrac{\tau_0}{\mu_0}\right)^n}{\dot{\gamma}}, & \text{if } \dot{\gamma} > \dfrac{\tau_0}{\mu_0} \end{cases} \tag{2.26}$$

3 Methodology

This section provides a description of how the study was set-up and various aspects pertaining to the computational model such as the domain, boundary conditions, discretization, and material definition of the slurry. The challenges faced while setting up the model as well as the workarounds used to mitigate these challenges are also briefly discussed.

3.1 Computational domain and boundary conditions

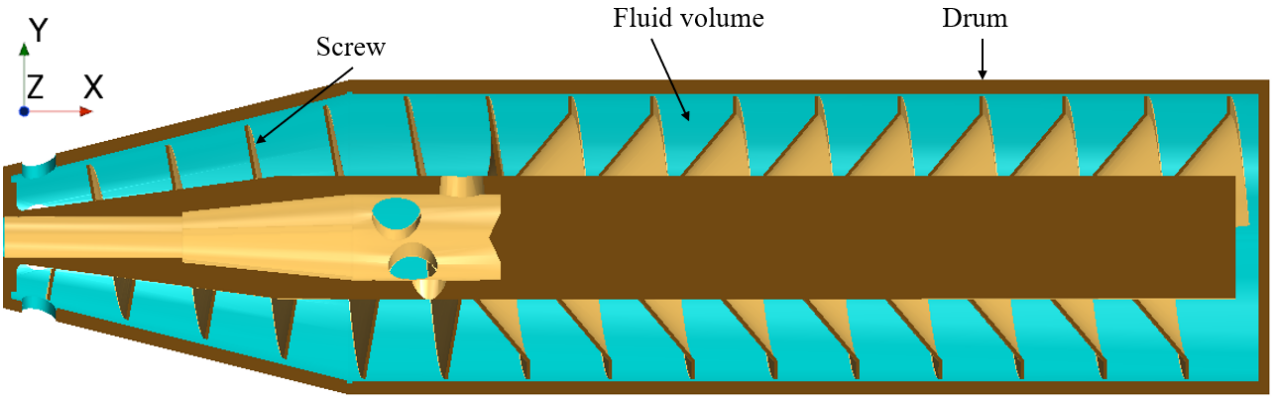

Figure 3.1: *CAD model showing a cut section of the decanter centrifuge studied*

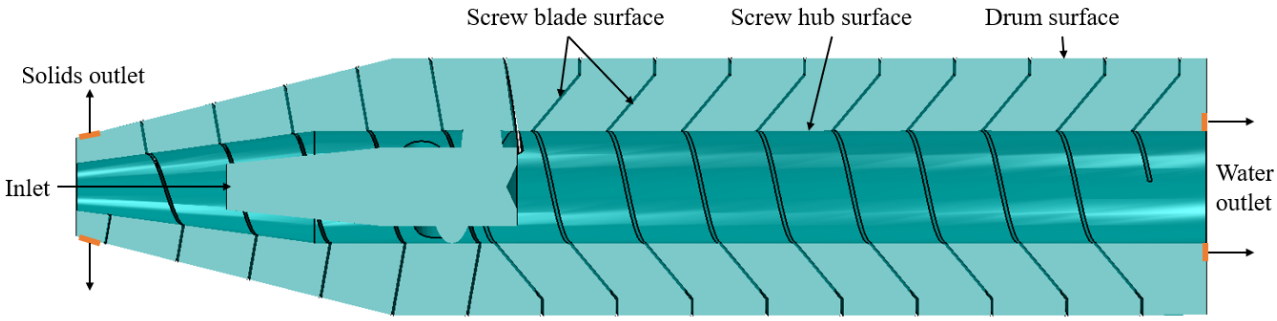

Figure 3.2: *Fluid volume extracted from the CAD model of the decanter*

Figure(3.2) shows the computational domain of this study which is the fluid volume present within the decanter centrifuge. Certain practical simplifications have been made to simplify the definition of certain boundary conditions and to avoid the use of mesh refinement in many places. These simplification and a general description of the computational domain along with the boundary conditions used are described below:

1. A decanter centrifuge is not a closed, air-tight system. It is open to the atmosphere at all of its outlets and all the void spaces within the machine are filled with air. The computational model does not consider air as a part of the system. Having air as the third phase would significantly increase the complexity of the simulation. A phase interaction between air and each of the other two phases would need to be defined. The free surface formed by air and mainly water towards the water outlet would require a more compressive scheme such as the Volume of Fluid (VOF) method to be resolved properly. The added complexity would not only make the computations much slower, but also increase the risk of ending up with an inaccurate representation of the

interaction between the three phases due to a lack of knowledge regarding these interactions.

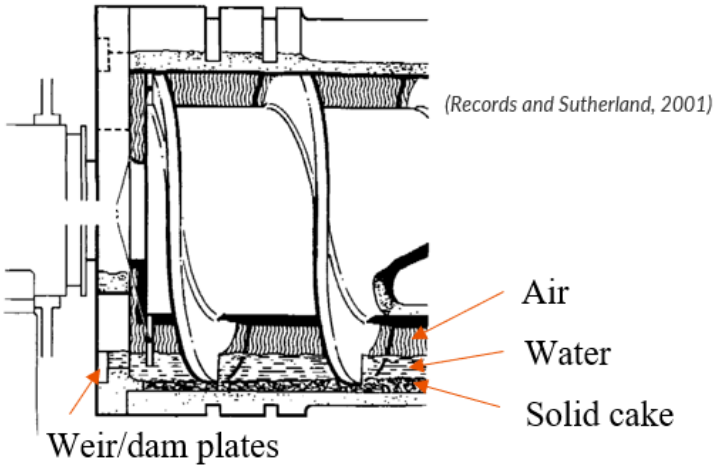

Figure 3.3: *Cut section of the decanter showing solid layer sticking to the drum and the free surface formed by water and air near the water outlet[2]*

2. Ideally, a pressure outlet boundary condition needs to be specified at the two outlets as they are open to the atmosphere and hence the pressure at these points is known. But this will only work if air is also taken into consideration in the computational model which is not the case. Setting a pressure outlet to the simplified model without air is not possible as the fluid pressure at the outlets cannot be determined. Using atmospheric pressure as the pressure is found to cause backflows and even divergence in some cases. Instead, the outflow boundary condition is applied at both the outlets which extrapolates the flow variables at the outlet surfaces by assuming a null-gradient with the neighboring cell. Although due to the presence of two outflow outlets, a volume split ratio needs to be specified for each outlet to ensure mass conservation. This split ratio is taken to be 1:9 for the cake and water outlets respectively based on experimental data provided by Noxon. The inlet on the other hand is quite straightforward. A mass flow inlet boundary condition with a specified volume fraction of each phase is used.

3. Both the solid and the water outlets in an actual decanter are just holes drilled into the drum. Although in the computational domain, they have been simplified to have an axis-symmetric geometry. This is done due to the way in which the differential speed between the drum and the screw is modelled by using a moving wall boundary condition on the drum surface. Having holes for outlets would mean having stationary holes on a moving wall which is nonphysical. An axis-symmetric geometry for the outlets is used to have a more physically realistic representation of the outlet. The area of these outlets is kept the same as the actual total area of the outlet holes.

4. A rotational speed differential between the drum and the screw is required to convey the solids up the conical section towards the solids discharge outlet. As explained in sec.(2.1.3), the sliding mesh approach is used in cases where the rotation can be applied to a part of the domain without actually creating a whole new mesh at every time-step. In this case, the entire domain can be rotated. This rotation is enough to ensure all the inertial forces such as centrifugal and Coriolis' forces are applied to the fluid as they should be. For the differential between the screw and the drum, either the screw can be rotated slower than the drum or the drum can be rotated faster than the screw. The former would again require modifying the entire mesh as the screw is not an axis-symmetric geometry. The latter can easily be achieved by just applying a

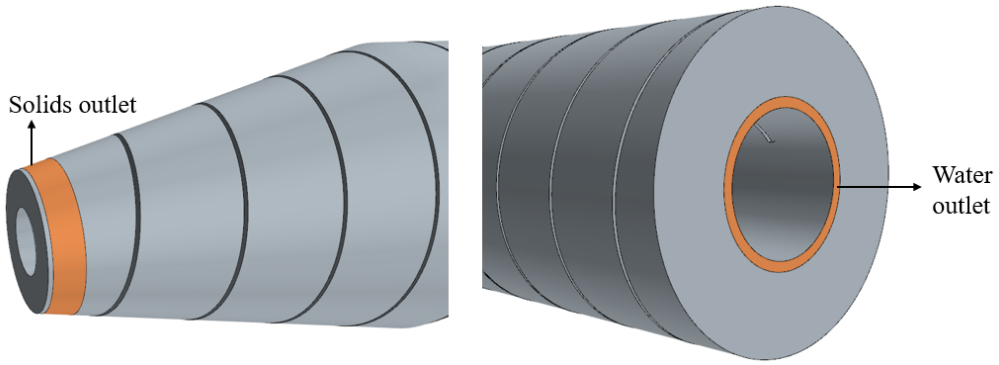

Figure 3.4: *Outlet geometry in the computational domain*

moving wall boundary condition at the surface of the drum. The motion applied in this case is rotation about the axis of the decanter. So the drum surface rotates a bit faster than the entire domain, hence simulating the effect of the differential speed (see fig.(3.5)). All the surfaces on the screw including the hub and blade surfaces, and the surface of the inlet chamber are modelled as no-slip walls having no relative velocity with respect to the rotating mesh. The drum surface is then modelled as a no-slip wall rotating 1.5 rad/s faster than the rotating mesh. This corresponds to the differential speed between the drum and the screw.

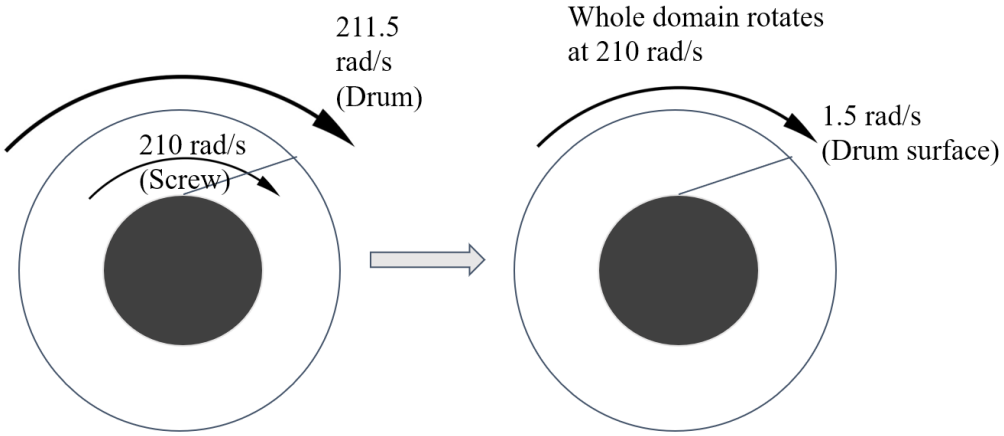

Figure 3.5: *Simplified sketch showing how the screw and the drum rotate in an actual decanter (left) and in the model that uses the sliding mesh approach along with a moving wall boundary condition (right).*

The use of the sliding mesh approach is not ideal as the transient simulations with small time steps is very time consuming. A pseudo-steady state moving reference frame (MRF) approach was the initial choice of model for the rotation. But the solver had some numerical issues in resolving the flow through using this technique. A lot of time and effort was spent on getting the steady state model to work but it did not come to fruition. In the end the transient sliding mesh approach had to be used to obtain some reasonable results.

5. In an actual decanter, there is a small clearance between the outer edge of the screw and the drum surface as these surfaces move at different speeds, this clearance is required to prevent wear due to the two surfaces rubbing against each other. However, a thin crust of solids is formed in this gap as it sticks to the surface of the drum. This solid crust has been found to

aid the conveying of the sedimented solids as the layer stuck to the surface prevents the solids from slipping around the screw[2]. The sticking of solids is thus encouraged through forming groves, using liners, or knurling the surface of the drum. Although for the computational model, these features along with the gap between the screw and the drum have been ignored. This is done to avoid using a fine mesh to capture the flow details in these regions and hence save on computational resources. Not having the clearance is equivalent to the solid crust having already been formed within the domain.

3.2 Discretization

The computational domain is dicretized in space using polyhedral cells. Polyhedral meshes provide a balance between computational time, and accuracy of the solution obtained[1]. Other mesh types such as tetrahedral and trimmed-cell mesher have certain drawbacks and hence were not of much interest in this case. Tetrahedral cells require 4-5 times more number of cells than polyhedral cells to achieve the similar levels of accuracy. Trimmed cell meshers work better with simpler geometries that contain almost flat surfaces aligned with the cartesian planes and do not contain narrow corners[1] which is not the case here.

In order to ascertain the right level of refinement required for the mesh and to strike a balance between accuracy of the solution and computational time required, a mesh dependency study is conducted wherein a particular simulation is run with multiple mesh refinement levels. It is made sure that all other settings remain same for all the cases. The simulation is run to simulate 4 seconds of physical time. Mass balance is used as measure of accuracy of each mesh.

For a steady state simulation, mass imbalance can directly be measured by checking the difference between total mass entering and total mass leaving the system. But for a transient simulation, as time goes on, some mass is also accumulated within the system or some mass that was present in the system initially starts flowing out of the system. This means that the difference between mass entering and leaving the system may not be zero at all times. The problem is exacerbated in multiphase flows where even minute numerical errors in calculating the volume fraction of each phase, add up over time to cause large amounts of inter-facial mass transfer even when there is supposed to be no mass transfer. The numerical error is measured seperately for each phase as well as for the entire mixture by substituting the corresponding mass flows in eqn.(3.1).

$$\text{Error} = (\dot{m}_{in} - \dot{m}_{out}) - \left(\frac{m_t - m_{t-1}}{\Delta t}\right) \tag{3.1}$$

Table 3.1: Comparison of different meshing strategies

Base cell size (m)	Number of cells	Timestep (s)	Error in mass w.r.t. inlet mass flow rate (%)	CPU hours required
0.0125	449082	0.0005	11.26	268.16
0.01	600527	0.0004	11.12	397.03
0.006	1372849	0.00028	11.08	1743.23
0.01 (with prism layers)	1044508	0.0004	28.81	405.55
0.01	600527	0.0002	6.85	580.69
0.01	600527	0.0001	3.09	937.58
0.02	172128	0.00005	1.19	1220.09

Errors in mass for the second phase for meshes with different levels of refinement, both in space and time are documented in table(3.1). 4 seconds of physical time is simulated for all the cases and the error measured is averaged over the last two seconds of the results. The first three meshes mainly differ in terms of the overall refinement of the mesh. The time-step is scaled to keep the courant number comparable in all three cases. Judging from the error in mass, it does not seem like the cell size has a great impact on the accuracy of the results. Although, due to the increasing number of cells, the computational time increases significantly. On the other hand comparing the results for cells with base size 0.01, but with different time steps, we see that the time step has a greater impact on accuracy. Having a coarser mesh but a lower time-step still results in a lower error as compared to the finest mesh with a higher timestep. Timestep appears to be playing a much significant role in the accuracy of the results as opposed to the base cell size.

Ideally, the whole simulation would be needed to run for much longer than 4 seconds to get a better judgement of the quality of mesh. But it is not possible to run so many cases for so long due to time constraints of the project. Although it is observed in the cases that were later run for over a 100 seconds that the level of error stays at around the same level as it is at 4 seconds, so it might just be enough to judge the error based on this short time period.

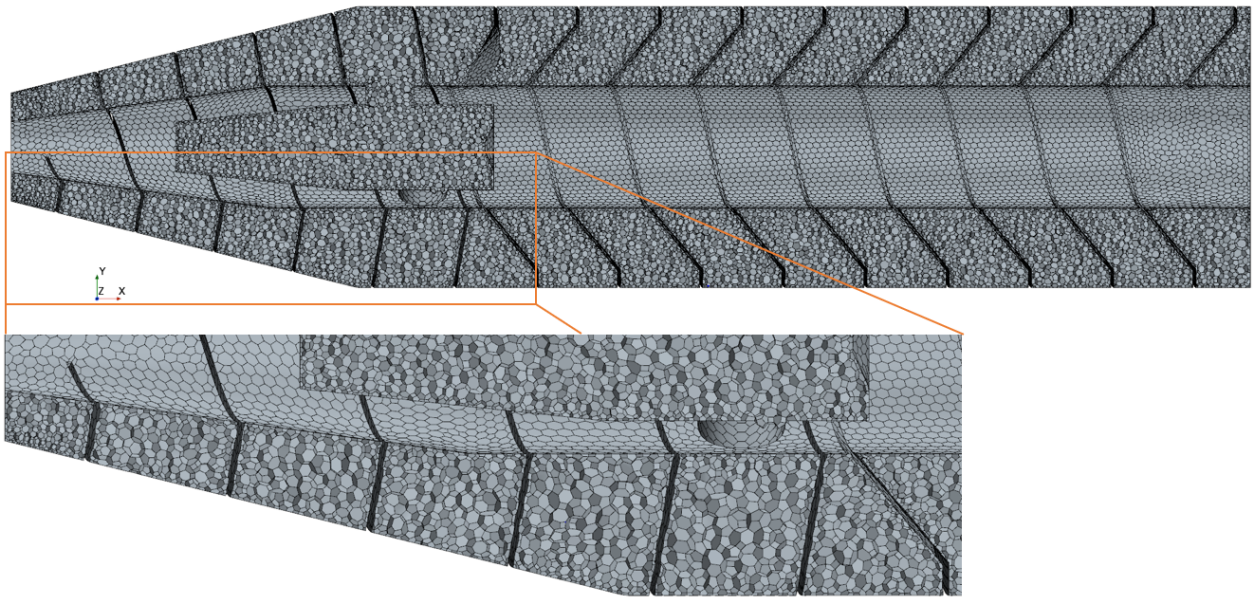

Figure 3.6: *Computational mesh*

2nd order discretization schemes are used for momentum, turbulent kinetic energy, and volume fraction. Since there were no numerical instabilities or convergence issues, no time was invested on testing first order schemes.

3.3 Material definition

The material definition of the slurry is the most crucial part of this project. The best way to provide an explanation for this part would be to provide a chronological account of the various material modelling approaches investigated. The following provides such a description of how the material modelling was done initially along with how and why it had to be modified due to certain issues arising through the course of the project.

Solid phase as particles

The study began with the most straightforward way of defining a material model for the slurry by modelling it as a two phase mixture of water and the solid phase, wherein the solid phase consisted of solid particles of a certain size distribution taken from experiments such as [3] and [22]. As mentioned in sec.(1.2.3), the non-newtonian rheology of the sludge is an important aspect which may have a significant impact on the flow. It is suggested in [1] that the 'suspension rheology model' from [23] is suitable for such flows where non-newtonian behaviour stems due to the solid volume fraction approaching the maximum packing fraction. This model has also been verified in [24] to give satisfactory results. Although we ran into a whole host of problems while using this approach. Firstly, we were forced to use the segregated eulerian multiphase model as the solver does not allow the specification of a solid phase with the simpler mixture multiphase model. But even with the segregated eulerian multiphase model, numerical instability was the biggest problem. We failed to achieve convergence even after multiple attempts, some of them on a simpler scaled down model to check for any faults in the modelling methodology. It can be speculated that this might be due to the improper definition of the inter-facial interaction due to lack of relevant data.

Solid phase as a dense and viscous liquid

Even though they are referred to as particles, the solid phase is in the form of irregularly shaped flocs, formed by the agglomeration of smaller individual particles. Due to the highly irregular shape of the flocs (fig.(3.7)), and the interactions among the flocs, the solid phase can be regarded to behave similar to a gelatinous material and less like a collection of solid particles. This meant that the solid phase now needed to be modelled as a dense and highly viscous liquid rather than solid particles. But now since both the phases were liquids, the mixture multiphase approach can be used which proved to be the solution to our convergence issues as well. Another advantage of this approach is that it allows the option of modelling the solid phase as a non-newtoninan fluid.

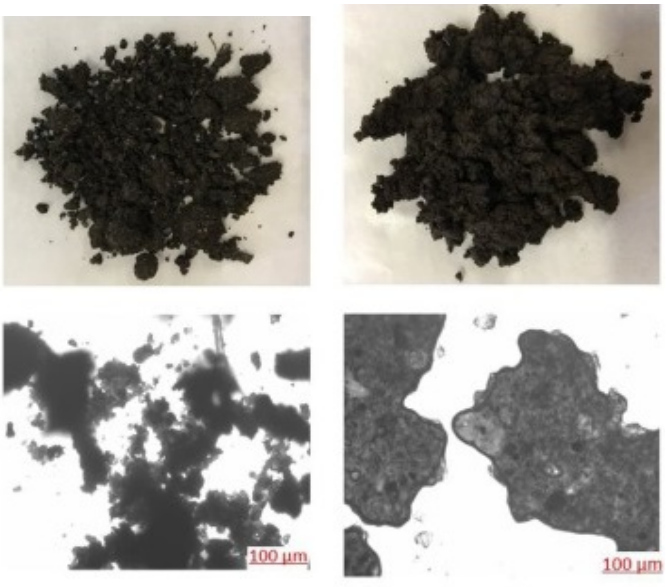

(a) (b)

Figure 3.7: *Appearance of the sludge flocs [3]*

Solid phase rheology

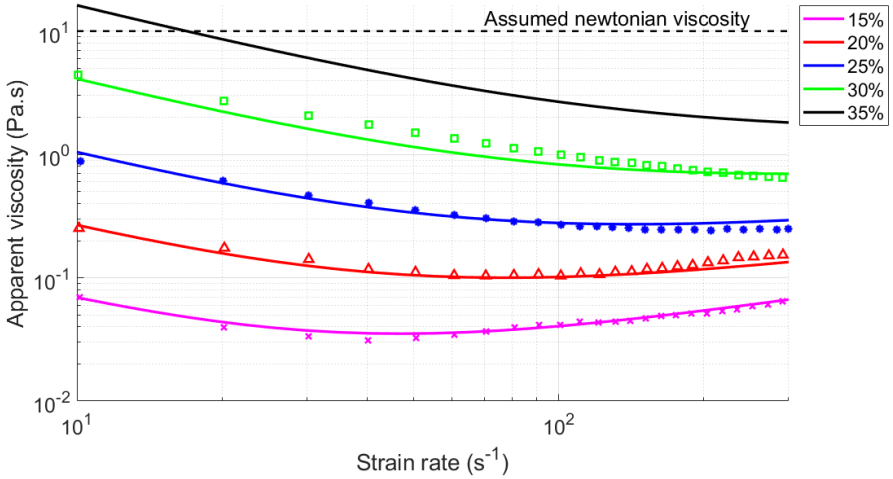

Figure 3.8: *Rheograms of dewatered sludge cakes with different solid concentrations[3]*

The rheology of the slurry depends heavily on the local solids concentration at that point. In the decanter, the solid concentration varies greatly from the inlet to the outlets. This means that the rheology also changes as the slurry flows through the decanter. The numerical solver works by taking a volume weighted average of material properties of both the phases present in a particular computational cell to calculate the corresponding properties for the mixture of phases. This means that the properties of the mixture in a cell lie somewhere between the properties of the constituent phases. This can be utilized to define the solid phase as the actual sludge cake that comes out of the solids discharge outlet of a real decanter. So in the computational model, the slurry is a two phase mixture of water and the sludge cake, where the properties of the sludge cake are defined according values obtained from experiments taken from [3].

The mixture-multiphase model uses the phase volume fraction for keeping track of the distribution of phases within the domain. This imposes an upper limit of 1 on the volume fraction of a phase. This is somewhat analogous to the values above 1 being clipped off. So in order to avoid this problem, the sludge cake is defined to have a higher solid concentration than the actual sludge cake. If it is assumed that the actual sludge cake has a TS of 25%, the model is considered to have a TS of 35%. In this way a volume fraction of 0.6803 for the modelled solid phase would correspond to a volume fraction of 1 for the actual sludge cake. This value is obtained based on mass balance calculations by assuming that all the solid that enters the domain is discharged only through the solids discharge outlet. All other properties like density, viscosity, inlet volume fraction etc. are scaled according to the new concentration.

Fig.(3.8) shows rheograms obtained from experiments performed on dewatered sludge cake samples with solid concentrations ranging from 15% to 30%. The points are taken from experiments and the lines are approximate curves that best fit the experimental data. This data is then used to extrapolate a rheogram for a sludge cake with solids concentration of 35%. The data pertaining to the slurry rheology is scarce and not so reliable due to reasons explained in sec.(1.2). Thus it is is better to treat these values as more of an approximation for a wide range of dewatered sludge cakes rather than exact values corresponding to any one particular slurry.

The solid phase is thus modelled as a thick liquid whose mechanical properties are extrapolated using data from experiments performed on sludge cakes obtained after dewatering. In order to avoid confusion, this phase will simply be referred to as the 'second-phase' from this point forward. So the computational model for the slurry is a two phase mixture of water and the second phase.

3.4 Case setup

After arriving at the final model, four cases were tested to study how the model behaves by varying different parameters. Four different cases were tested, and the parameters that varied among them are the viscosity and mass flow rates. All other parameters remain constant in all four cases. All cases were initialized with water in the whole domain. The cases are transient simulations that ran for 100 seconds, with a time step of 0.00005 seconds. The boundary conditions for the base case have been tabulated in table(3.2) (refer fig.(3.2) for the locations of the boundary conditions) and the setup of the four cases tested is summarized in table(3.3).

Table 3.2: Boundary conditions for the base case

Location	**Type**	**Parameter**	**Value**
Inlet	Mass flow inlet	Total Mass flow rate	5.08 kg/s
		Volume fraction of water	0.9088
Solids outlet	Outflow	Split ratio	0.1
Water outlet	Outflow	Split ratio	0.9
Drum surface	Wall	Local rotation rate	1.5 rad/s
		Shear stress specification	No-slip
Screw blade surface	Wall	Stationary wall	-
		Shear stress specification	No-slip
Screw hub surface	Wall	Stationary wall	-
		Shear stress specification	Slip

Table 3.3: Summary of the different cases tested

Case	**Case name**	**Specification**
1.	Base	Base case with a dynamic viscosity of 10 pa.s for the second phase (newtonian rheology) and a inlet mass flow rate of 5.08 kg/s
2.	Low viscosity	Dynamic vsicosity in the base case lowered to 1 pa.s
3.	Non-newtonian	Non newtonian rheology for the second phase with parameters: K= 0.64, n=1.1247, τ_0=153.6 Pa, $\mu_0 = 16.2115 Pa.s$
4.	High mass flow rate	Mass flow rate 1.5 times that of the base case ie. 7.62 kg/s

4 Results and Discussions

The final results from the study are presented in this section. Different methodologies such as the MRF approach, the suspension rheology model, the segregated eulerian multiphase flow model etc. were initially considered for the model but in the end could not be investgated further due to certain shortcomings associated with them which are explained throughout chapter(3). The results from those investigations form an important part of the modelling process but are not relevant to the final model and thus have not been presented in this report. The results presented in this section pertain to the model described in chapter(3). The case setup is described in sec.(3.4).

4.1 Results for the base case

The volume fraction of a particular phase basically shows its distribution in the domain. In order to see how the model has performed in separating the two phases, we can take a look at the volume fraction of the second phase.

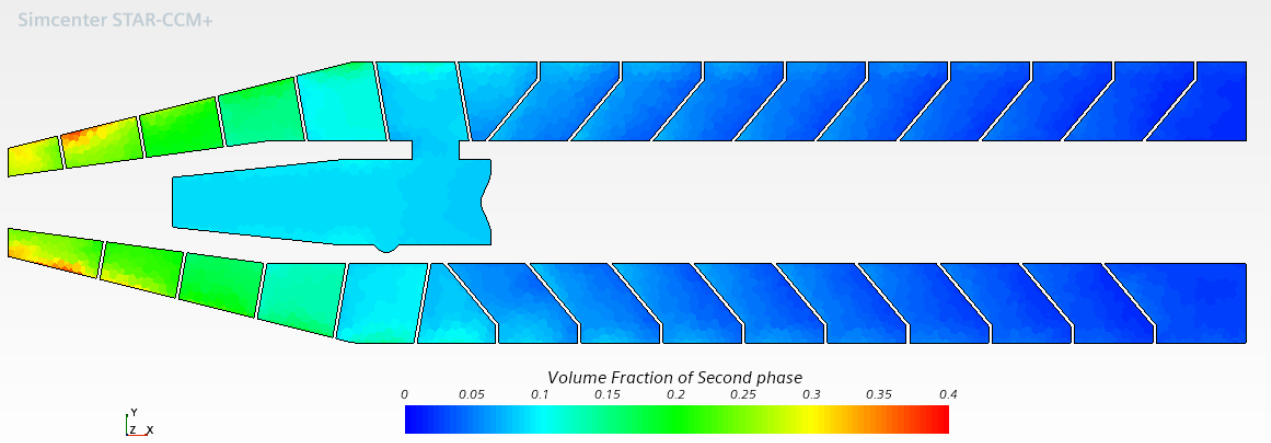

Figure 4.1: *Second phase volume fraction contour plot on a plane section passing through the centre of the decanter.(Base case at 100 seconds)*

It is clearly seen in fig.(4.1) that the volume fraction of the second-phase is higher towards the tapered section of the decanter. This is in line with the working principle of the decanter that the solids are conveyed up the tapered section and compacted. This compaction can be seen as an increase in the volume fraction of the second phase which is a counter part to a dense mixture of solids and water. To get a clearer picture, we can take a look at fig.(4.2) that shows the evolution of this volume fraction with time. We also see compaction to a certain extent as the volume fraction increases as we move leftwards towards the solids discharge outlet. On the other hand, from fig(4.1), the volume fraction decreases as we move right towards the water outlet. Which means the water becomes cleaner as we move further away from the inlet holes. Figure.(4.3) shows the distribution of the second phase over the two outlets. There is a clear difference in the volume fraction of second phase between the solids discharge outlet (cake outlet) and the reject water discharge outlet(water outlet). These figures are enough to show that the model of the decanter is qualitatively doing what it should, ie. increase the concentration of each phase at their respective outlets.

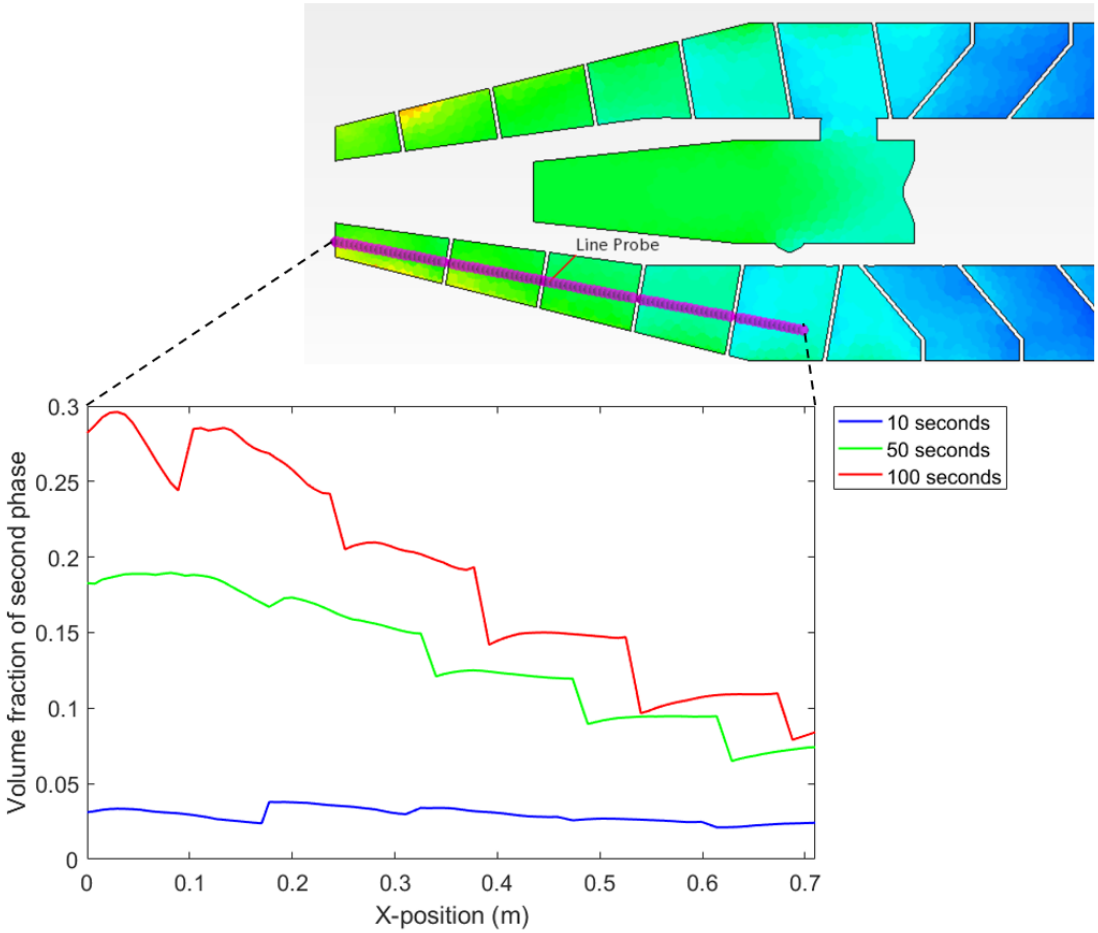

Figure 4.2: *Evolution of second phase volume fraction with time along a line probe through the tapered section of the decanter (Base case)*

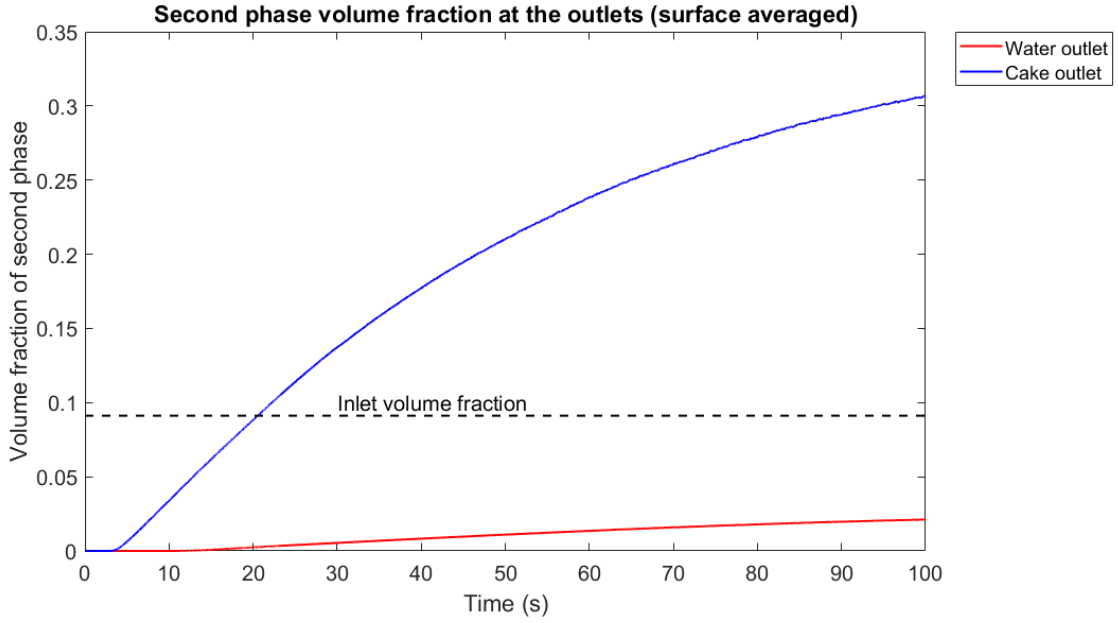

Figure 4.3: *Surface averaged second phase volume fraction at the outlets vs. time (Base case)*

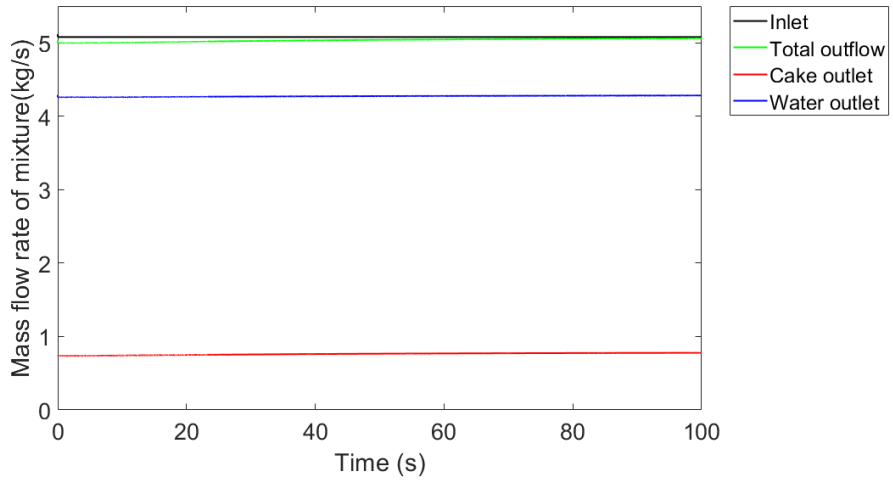

(a) *Mixture*

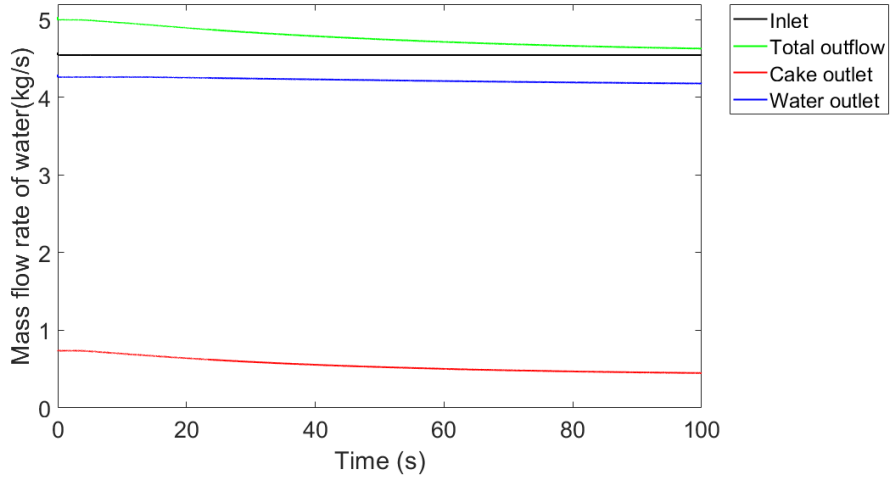

(b) *Water*

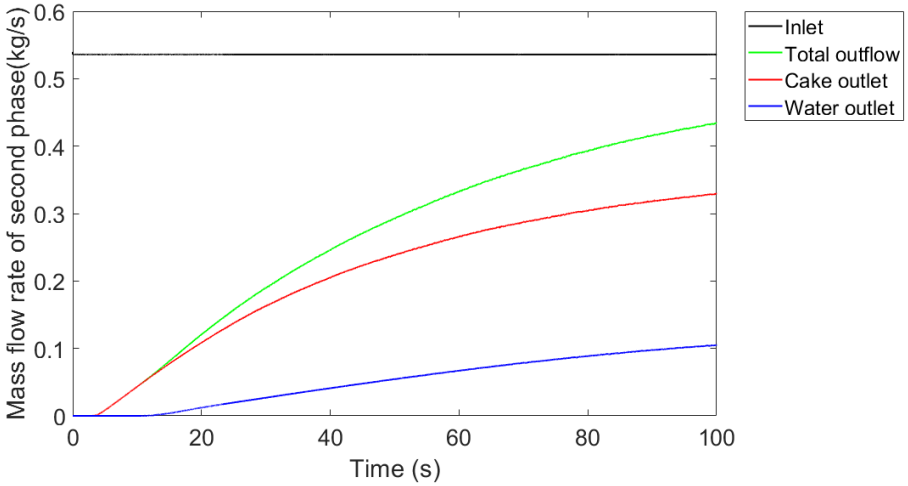

(c) *Second Phase*

Figure 4.4: *Mass flow rate for the (a) Mixture, (b) Water, and (c) Second phase at different locations*

Figure(4.13) is an extension to fig.(4.3). It shows the mass flow rate at the inlet and the outlets for each phase as well as for the entire mixture. The mass flows in and out of the domain in fig.(4.4a) show the overall mass conservation is reasonably satisfied . From figs.(4.4b) and (4.4a), the accumulation of the second phase within the domain becomes quite clear as the inflows and total outflows do not match. As the second phase accumulates in the domain more water is also being pushed out of the domain ensuring continuity. There is a difference in inflows and outflows also because steady state has not been reached as only 100 seconds of physical time were simulated due to time constraints associated with the project.

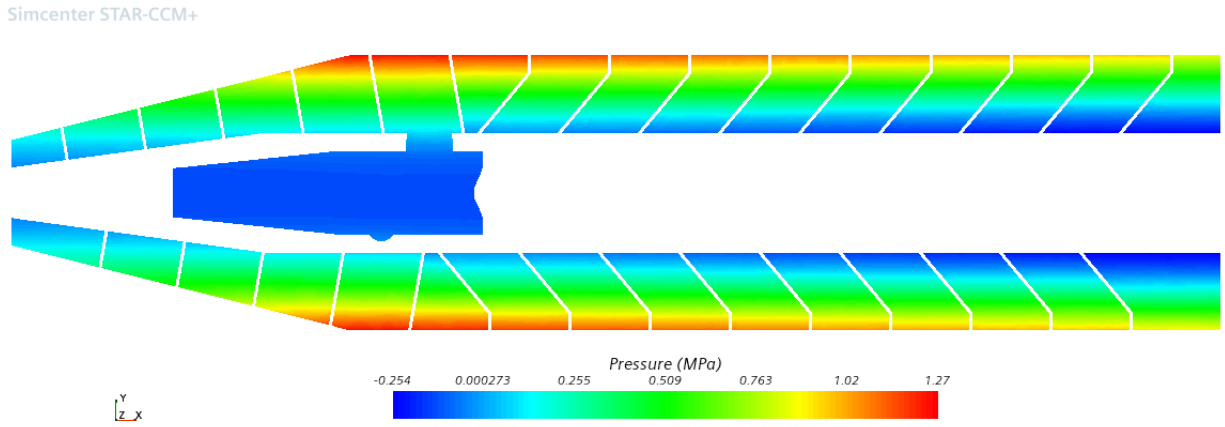

Figure 4.5: *Pressure contour plot on a plane section passing through the centre of the decanter.(Base case at 100 seconds)*

The pressure contour shown in fig.(4.5) can also be used to make a qualitative judgement about the model. It is clear from the pressure contour that pressure is increasing in the radially outward direction. This can be attributed to the centrifugal force which also increases as we move radially outward. It is this centrifugal force that is responsible for the separation of the two phases. There is a part of the domain where the pressure is negative. This can be interpreted as a result of the absence of air in this system.

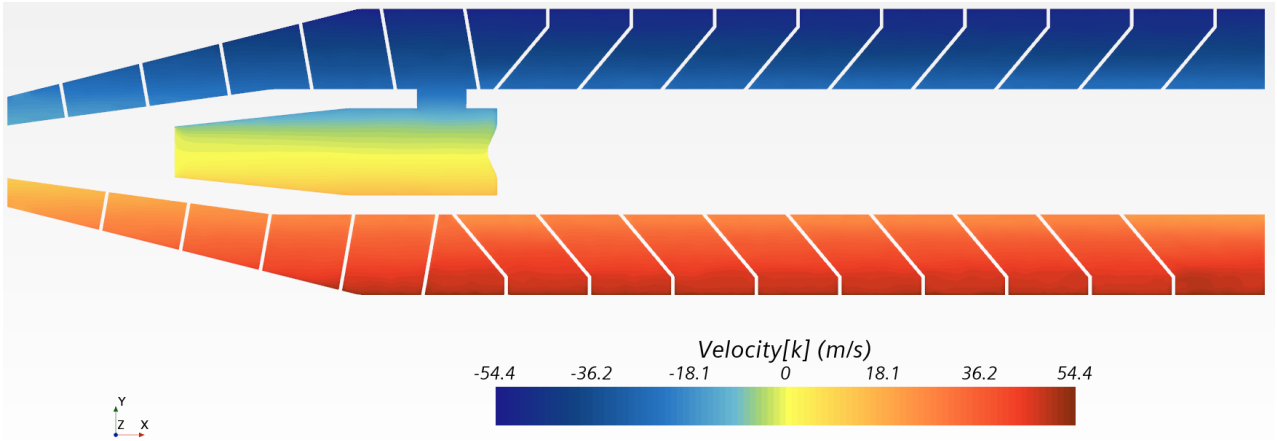

Figure 4.6: *Z or tangential Velocity component in the absolute frame of reference(Base case at 100 seconds)*

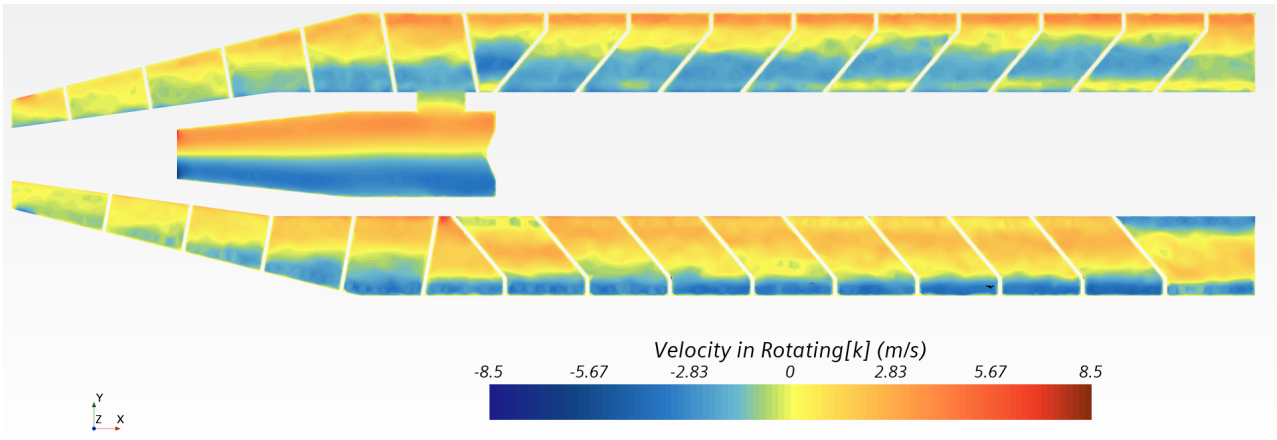

Figure 4.7: *Z or tangential Velocity component in a frame of reference rotating with the decanter(Base case at 100 seconds)*

The tangential velocity contour shown in fig.(4.6) is plotted with respect to the absolute frame of reference. The velocity appears to be directly proportional to the radius as expected (with the rotational speed being the constant of proportionality). But to get a better picture of the flow we need to take a look at this velocity in a rotating frame of reference with a rotational speed that matches that of the sliding mesh. We see a clear zone of fluid with a relatively higher tangential velocity magnitude close to the drum wall. This high velocity zone is probably formed due to the moving wall boundary condition at the drum wall. The second phase under the action of the centrifugal force gets pushed towards the drum wall and ends up in this zone of higher velocity. The moving drum surface and no-slip condition on that wall push the fluid against the helical screw surface. In this way the second phase is being transported towards the tapered end in the model.

4.2 Different viscosities for the second phase

As discussed in sec.(1.2.3), the slurry being analysed here is known to exhibit a non-newtonian rheology. This impact of the non-newtonian behaviour on the flow characteristics within the decanter may be important. In order to find out if that is the case, a case was run by altering the rheology of the second phase according to rheological measurements conducted on a similar solid sludge cake. To further assess the impact of viscosity on the flow field, an additional case was also run with a much lower Newtonian viscosity compared to the base case. The exact case setups have been summarized in tab.(3.3) and the results are presented here. Figures (4.9),(4.10), (4.8) and (4.11) show the comparison of various variables among the three cases tested.

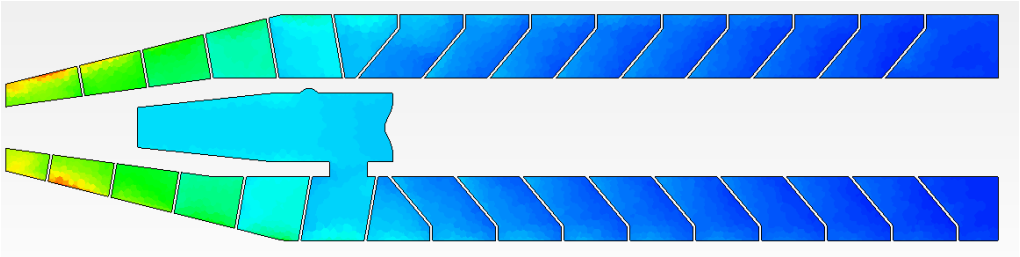

(a) *Base*

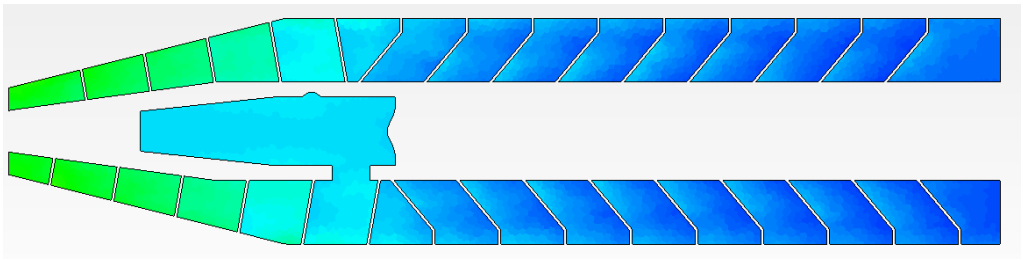

(b) *Low viscosity*

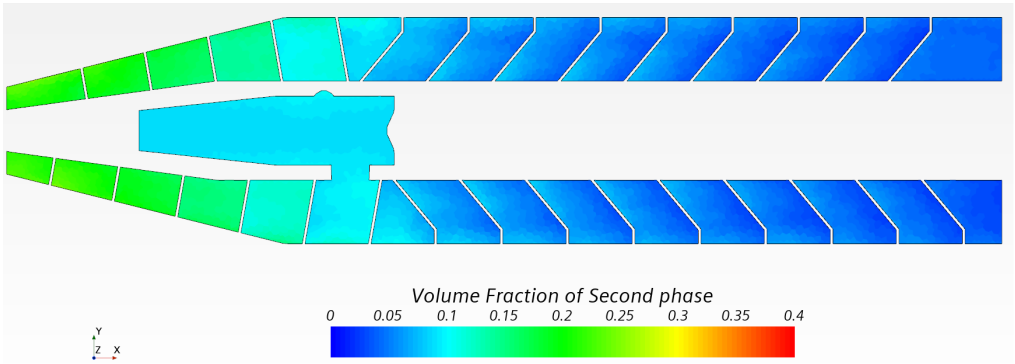

(c) *Non-newtonian*

Figure 4.8: *Second phase volume fraction contour plots for (a) Base, (b) Low-viscosity, and (c) Non-Newtonian cases at 100 seconds of solution time*

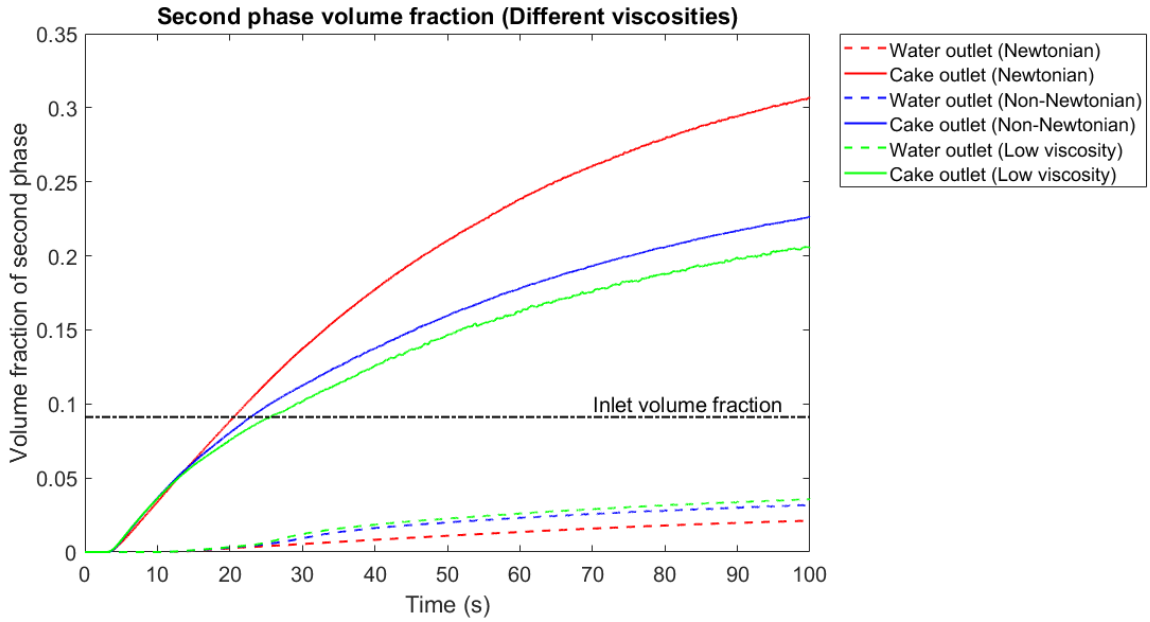

Figure 4.9: *Surface averaged second phase volume fraction at the outlets vs. time for the three cases*

One detail that stands out among these cases is the similarity between the low-viscosity and the non newtonian cases. This similarity can give an indication that the non-newtonian rheology or at-least some aspects of it do not influence the flow in a considerable way. This would mean that the flow could be modelled using a newtonian fluid but with a better approximation for its viscosity so that it is as close to the non-newtonian fluid as possible. Doing so would cut down the number of parameters from four namely the power law index, consistency factor, yield stress, and yielding viscosity to just one i.e. the dynamic viscosity. In the current study, the low viscosity and the

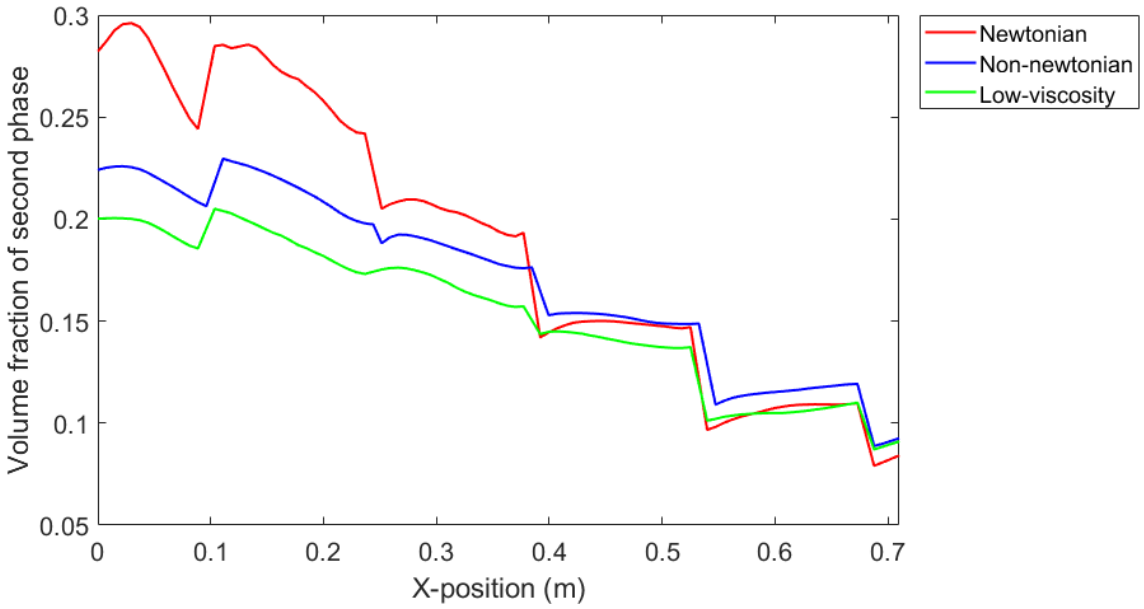

Figure 4.10: *Second phase volume fraction through the line probe shown in fig.(4.2) at 100 seconds of solution time, for the three cases*

non-newtonian cases were run simultaneously and the value of viscosity for the low viscosity case was guessed just to see its impact on the flow. But with the knowledge from these cases, a value of viscosity closer to the non newtonian value could be tested but has not been done due to the time constraints.

The torque curves shown in fig.(4.11), are only indicative and are used as a means to compare the various cases. The values of torque obtained here will not be the same as the actual measured values in such a decanter due to the numerous simplifications to the computational model. In an actual

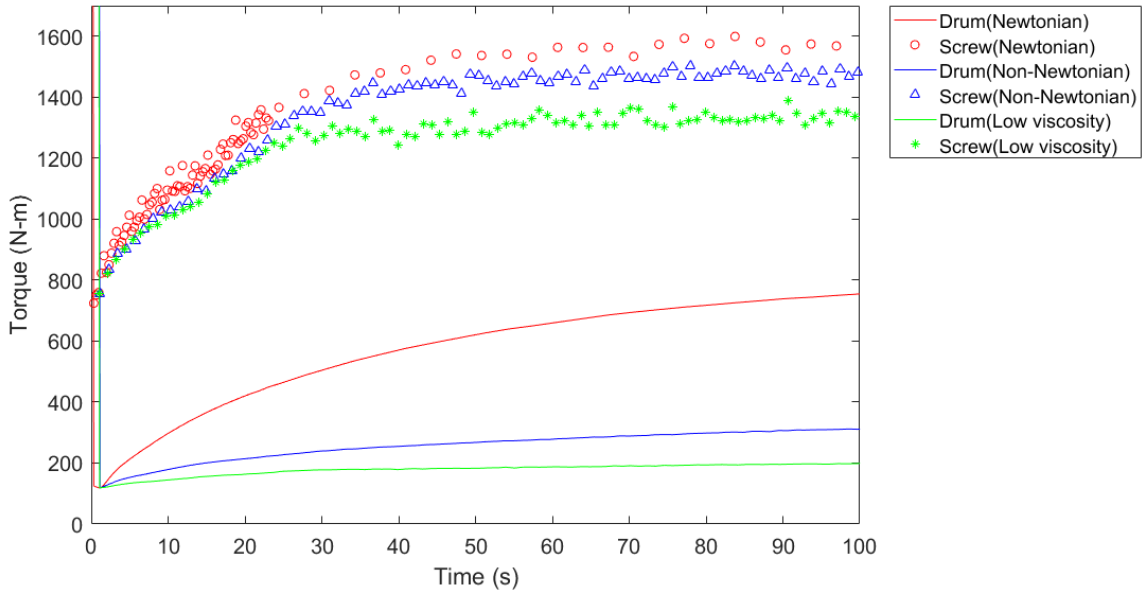

Figure 4.11: *Torque on the screw and drum surfaces vs. time for the three cases*

decanter, the total torque is a contribution from different contributions such as the torque to overcome friction, convey the solids up the conical end, accelerate the axially incoming feed into the tangential direction etc.[25]. Many of these contributions are not taken into account in the computational model, so it cannot be used as a validation parameter for this model.

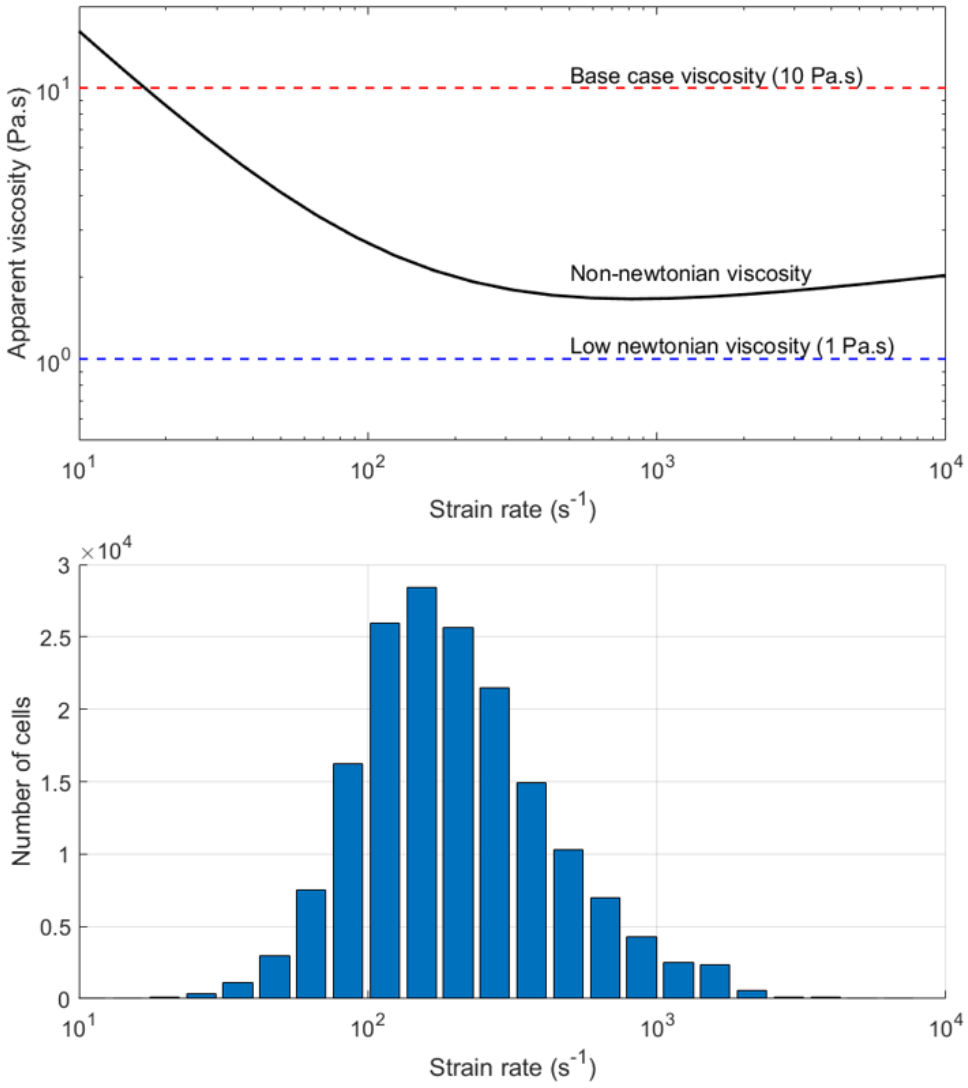

Figure 4.12: *Rheogram showing the viscosities on top and the strain rate histogram for the whole domain for the non-newtonian case*

One possible reason for the similar behaviour of the non-newtonian and low-viscosity cases can be explained using fig.(4.12). The graph in the top of the figure shows a rheogram with all the three viscosities plotted against strain rate. The plot on the bottom shows a histogram of the strain rate in all the cells present in the domain for the non-newtonian case. It is is clear from the histogram that a very small number of cells have quite small values of strain rate occurring in them, and majority of the cells have a strain rate magnitude between 50 and 1000 s^{-1}. Looking at this region in the histogram, it is way past the viscoplastic regime of the rheogram (close to 10 s^{-1}). The non–newtonian viscosity in this region, although not exactly constant, does not vary significantly either. So this further points towards the possibility of assuming the slurry as Newtonian to make the model a whole lot more simpler while impacting the results marginally. These results however only give an indication as to

how the computational model is working and thus should not be taken as the final conclusion as they could not be validated against experimental results due to practical difficulties as discussed in chapter(3).

4.3 Higher mass flow rate

Another interesting parameter that was tested is the mass flow rate of the slurry flowing through the decanter. The mass flow rate considered in the base case is the usual operating range of the machine modelled here. According to Noxon, the machine is known to start push out the incoming slurry out of bearing seals and any gaps present around the inlet chamber when a relatively high mass flow rate of slurry is fed to the decanter. The reason behind testing a higher mass flow rate is to see if any information can be gathered from the results about the cause of this overflow behaviour.

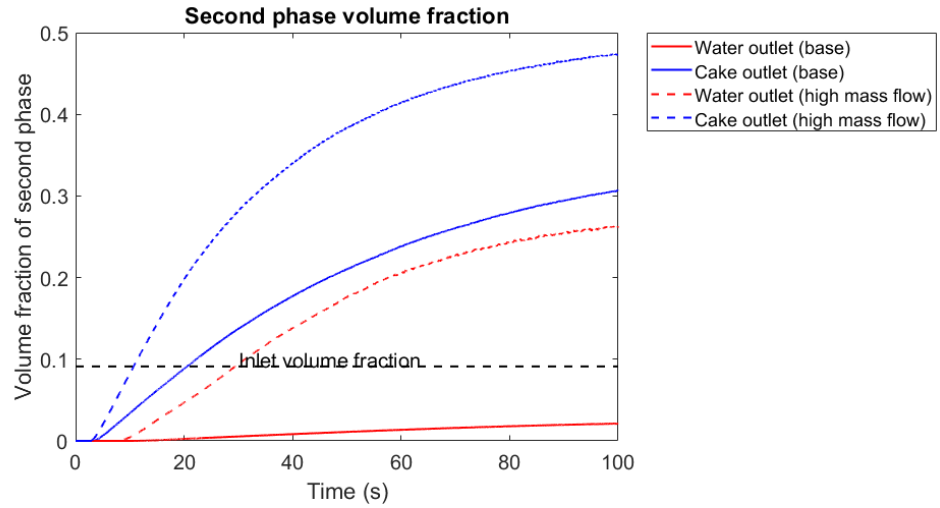

(a) *Surface averaged second phase volume fraction at outlets*

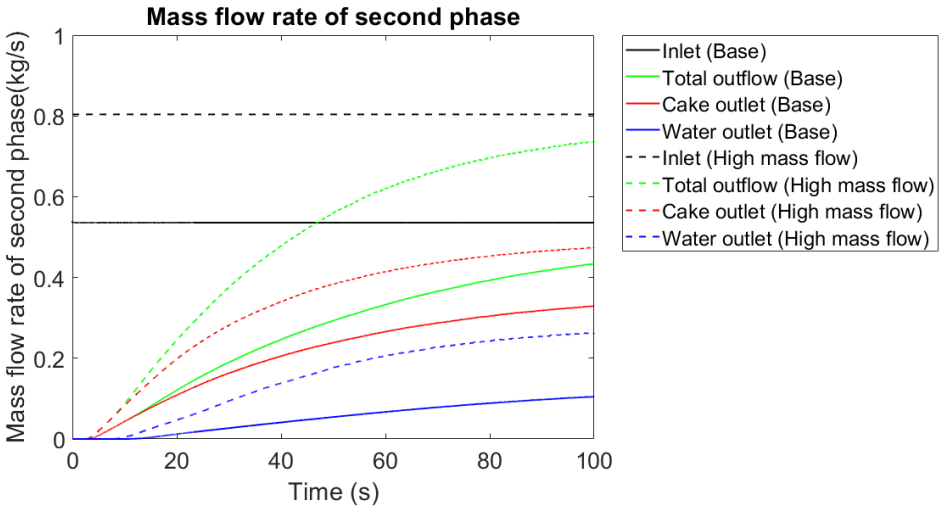

(b) *Mass flow rate at outlets*

Figure 4.13: *Comparison between the base and high mass flow cases based on (a) Outlet volume fraction and (b) Mass flow rates at inlet and outlets.*

Unfortunately, no conclusive trend can be seen from the results of this case. Figure(4.13a) does indicate a substantially higher volume fraction at the water outlet but is also contradicted by a higher volume fraction at the cake outlet. Similar trends are also seen in fig.(4.13b). These inconclusive results definitely do not indicate the cause of the overflow behaviour encountered in real life. This can also be due to the fact that air has been ignored in this study. The slurry is pressed out of the openings in the machine that are open to the atmosphere and due to the simplifications made to the computational model, no judgement can be made about the interaction of the slurry with the air.

5 Conclusion and Future Scope

5.1 Conclusion

The work presented in this master's thesis gives an overview of the CFD modelling of the flow inside an industrial decanter centrifuge used to seperate bio-solids and water from municipal sewage sludge. The development of such a model would reduce the dependency on unreliable and expensive experimental work needed to study the flow inside a decanter centrifuge.

The sewage slurry modelled here was known to exhibit viscoplasticity, shear-thinning, and thixotropic behaviour. In addition to certain solver limitations, the experimental data regarding the mechanical properties of such a slurry was scarce and unreliable and hence suitable simplifications were made to the material model. The slurry was hence modelled as a two phase mixture of water and a highly viscous and dense fluid acting as a counterpart to the dense mixture of solids and water. The rheological data for this second phase is taken from experiments conducted on sludge cake samples gathered after dewatering. Segregated and mixture multiphase flow models were investigated for solving the multiphase flow field. The segregated multiphase model had convergence issues and thus had to be shelved. The mixture multiphase model had the advantage of being simpler and robust and was hence chosen to solve the flow.

The motion of the decanter was modelled using a sliding mesh approach. The rotation of the entire decanter drum generates the centrifugal force necessary to sediment out the solid phase from the water. Then the relative motion of the screw and the drum is what conveys the solids out of the decanter. Initially the MRF pseudo steady state approach was investigated as it would have reduce the computational effort required for the calculations significantly. Although in principle, this approach should have worked for modelling the flow, it did not seem to faithfully model the centrifugal forces which are an integral part of this flow. As a result the switch to the transient sliding mesh approach had to be made wherein the whole mesh rotates with the desired rpm. The relative motion between the screw and the drum is modelled using a moving wall boundary condition on the drum surface. Switching to the sliding mesh approach made the calculations substantially slower as it is a transient approach. In addition to this, it was also noted that a very fine timestep is required to obtain satisfactory levels of phase-mass conservation and hence only a limited physical time was able to be tested for a limited number of cases.

The results could not be validated due to lack of relevant experimental data and also due to the numerous modelling simplifications made but the results are in qualitative agreement with the expectations. With the developed model, four test cases were run. The first three cases differed from each other in terms of the viscosity used of the second phase. The base case had newtonian viscosity of $10 Pa.s$ (this is the base case), the second case had a viscosity of $1 Pa.s$ and the third had a non newtonian second phase. The comparison among these three showed that the non-newtonian case did not differ considerably from the low-viscosity, newtonian case. The strain rate magnitude in the domain indicated that most of the cells had strain rate magnitudes much higher than the viscoplastic region of the slurry considered. This pointed towards the non-newtonian behaviour being of not so much importance to the model. Although experimental validation would be required to further solidify this argument. The final test case had a higher inlet mass flow rate compared to the base case. Although this case did not give any conclusive results.

The model presented in this project was an attempt to model the flow inside a decanter centrifuge to as great an extant as possible. The presence of the relative motion between the screw and the drum, and the complex slurry rheology made the modelling quite complicated. The solver also presented

some limitations and some unforeseen shortcomings which costed a lot of time and effort. In the end the model that was developed, does to some extent, model the flow in a decanter centrifuge but its validity is yet to be tested through experimental validation.

5.2 Future Scope

The following is a list of things that could be studied or implemented in the future which for one reason or the other could not be a part of this project.

- The current solver did place limitations on the use of the solid phase with the mixture multiphase model as well as led to convergence issues with the segregated eulerian model and MRF approach. This can be due to how these models are implemented within the solvers code and so another solver might work better in this case.
- Experimental validation is must for any computational model. That being said, there is a severe lack of data regarding the flow through a decanter centrifuge. The availability of such data could enable experimental validation in the future making the model more reliable.
- Further validation of the results showing indicating non-newtonian behaviour to not have a considerable impact on the flow. This would cut down the number of unknowns and make both experimental and computational analysis of such a system simpler.
- The study of the interaction of air with the slurry, especially in the inlet chamber would provide a better picture of the overflow phenomena encountered by the machine at higher mass flow rates. But a three phase study would be much more complicated than the already quite complex two phase flow.

A Appendix

A.1 Diffusive flux

The discretized diffusive term is written as:

$$D_f = (\Gamma \nabla\phi \cdot \mathbf{a})_f \tag{A.1}$$

In order to obtain an accurate second-order estimation for the gradient at the face that implicitly involves the neighbouring cell values ϕ_0 and ϕ_1, the following relations are used:

$$\nabla\phi_f = (\phi_1 - \phi_0)\vec{\alpha} + \overline{\nabla\phi} - (\overline{\nabla\phi} \cdot \mathbf{ds})\vec{\alpha}$$
$$\vec{\alpha} = \frac{\mathbf{a}}{\mathbf{a} \cdot \mathbf{ds}}$$
$$\mathbf{ds} = \mathbf{x_1} - \mathbf{x_0}$$
$$\overline{\nabla\phi} = \frac{\nabla\phi_0 + \nabla\phi_1}{2}$$
$$\text{Hence,} \quad D_f = \Gamma_f \Big[\big(\phi_1 - \phi_0\big)\vec{\alpha} \cdot \mathbf{a} + \overline{\nabla\phi} \cdot \mathbf{a} - (\overline{\nabla\phi} \cdot \mathbf{ds})\vec{\alpha} \cdot \mathbf{a} \Big] \tag{A.2}$$

A.2 Convective Flux

The discretized convective term is written as:

$$(\rho\phi\mathbf{v} \cdot \mathbf{a})_f = (\dot{m}\phi)_f = \dot{m}_f\phi_f \tag{A.3}$$

Where, ϕ_f indicates the cell face value of a general variable ϕ. In order to calculate this term, a second order upwind scheme is used based on the linear interpolation of neighbouring cell face values denoted by 0 and 1.

$$(\dot{m}\phi)_f = \begin{cases} \dot{m}_f\phi_{f,0} & \text{for } \dot{m}_f \geq 0, \\ \dot{m}_f\phi_{f,1} & \text{for } \dot{m}_f < 0 \end{cases}$$
$$\text{Where,} \quad \phi_{f,0} = \phi_0 + \mathbf{s_0} \cdot (\nabla\phi)_{r,0} \quad \textit{and} \quad \phi_{f,1} = \phi_1 + \mathbf{s_1} \cdot (\nabla\phi)_{r,1}$$
$$\text{With,} \quad \mathbf{s_0} = \mathbf{x_f} - \mathbf{x_0} \quad \textit{and} \quad \mathbf{s_1} = \mathbf{x_f} - \mathbf{x_1}$$

The gradients are calculated using as limited reconstruction gradients using the following relations:

$$(\nabla\phi)_{r,0} = \alpha\nabla\phi_0$$
$$\phi_0^{\max} = \max(\phi_0, \phi_{\text{neighbours}})$$
$$\phi_0^{\min} = \min(\phi_0, \phi_{\text{neighbours}})$$
$$\Delta_{\max} = \phi_0^{\max} - \phi_0$$
$$\Delta_{\min} = \phi_0^{\min} - \phi_0$$
$$\Delta_f = \phi_{f,0} - \phi_0 = \mathbf{s}_0 \cdot (\nabla\phi)^u_{r,0}$$
$$r_f = \begin{cases} \dfrac{\Delta_f}{\Delta_{max}} & \text{for } \Delta f > 0, \\ \\ \dfrac{\Delta_f}{\Delta_{min}} & \text{for } \Delta f \leq 0, \end{cases}$$
$$\alpha_f = \frac{2r_f + 1}{rf(2r_f + 1) + 1}, \quad \alpha = min(\alpha_f)$$

A.3 Grid flux

This term is defined based on the volume swept δV_f, by face f, in time Δt due to the motion of the mesh. Using a second order approximation in time, G is calculated as follows:

$$G = \frac{(\alpha^2 - 1)\delta V_f^{n+1} - \delta V_f^n}{\alpha(\alpha - 1)\Delta t^{n+1}} \tag{A.4}$$

$$\text{where,} \quad \alpha = 1 + \frac{\Delta t^{n+1}}{\Delta t^n} \quad \Delta t^{n+1} = t^{n+1} - t^n \quad \Delta t^n = t^n - t^{n-1}$$

A.4 Turbulence

There are numerous coefficients associated with the turbulence model used. The definition of these coefficients for the realizable $k - \epsilon$ model is given below:

1. Curvature correction factor f_c : is used in the $k - \epsilon$ model to incorporate the stabilizing and destabilizing effects strong streamline curvature and frame rotation. The curvature correction factor alters the TKE production according to the local rotation and vorticity values.

$$f_c = min\left(C_{max}, \frac{1}{C_{r1}(|\eta| - \eta) + \sqrt{1 - min(C_{r2}, 0.99)}}\right) \tag{A.5}$$

$$\text{Where} \quad \eta = T^2(\mathbf{S} : \mathbf{S} - \mathbf{W} : \mathbf{W}) \quad \text{and,} \quad T = max\left(\frac{\varepsilon}{k}, \left[\left(\frac{\varepsilon}{k}\right)^{1.625} 6\sqrt{\frac{\nu}{\varepsilon}}\right]^{\frac{1}{1.625+1}}\right)$$

2. Damping functions f_μ and f_2 : are damping coefficients used to prevent nonphysical behaviour by enforcing certain mathematical constraints on the normal stresses [13][1]. This concept is known as realizability

$$f_\mu = \left[C_\mu\left\{4 + \sqrt{6}cos\left[\frac{1}{3}cos^{-1}\left(\sqrt{6}\frac{\mathbf{S}^{*3}}{\sqrt{\mathbf{S}^* : \mathbf{S}^{*3}}}\right)\right]\frac{k}{\varepsilon}\sqrt{\mathbf{S} : \mathbf{S} + \mathbf{W} : \mathbf{W}}\right\}\right]$$

$$f_2 = \frac{k}{k + \sqrt{\nu\varepsilon}}$$

$\mathbf{S}$ is the strain rate tensor as defined earlier and $\mathbf{W}$ is the vorticity tensor with magnitude W.

$$\mathbf{W} = \frac{1}{2}(\nabla\overline{\mathbf{v}} - \nabla\overline{\mathbf{v}}^T)$$
$$W = |\mathbf{W}| = \sqrt{2\mathbf{W} : \mathbf{W}^T}$$
$$\mathbf{S}^* = \mathbf{S} - \frac{1}{3}tr(\mathbf{S})\mathbf{I}$$

3. Other model coefficients and their values:

Table A.1: Model coefficient values for the realizable $k-\varepsilon$ model

Model Coefficient	Value
σ_k	1
σ_ε	1.2
$C_{\varepsilon 1}$	$\max(0.43, \frac{\eta}{5+\eta})$, where $\eta = \frac{Sk}{\varepsilon}$
$C_{\varepsilon 2}$	1.9
C_μ	0.09
C_t	1

References

[1] Siemens Digital Industries Software, "Simcenter STAR-CCM+ User Guide v. 2021.1," Siemens 2021.

[2] A. Records and K. Sutherland, "Preface and acknowledgements," in *Decanter Centrifuge Handbook* (A. Records and K. Sutherland, eds.), pp. xiii–xv, Amsterdam: Elsevier, 2001.

[3] S. Y. Edifor, Q. D. Nguyen, P. van Eyk, P. Biller, and D. M. Lewis, "Rheological studies of municipal sewage sludge slurries for hydrothermal liquefaction biorefinery applications," *Chemical Engineering Research and Design*, vol. 166, pp. 148–157, 2021.

[4] F. F. Andreoli C. V., von Sperling M., "Sludge treatment and disposal," in *Biological Wastewater Treatment Series*, IWA Publishing, 2007.

[5] P. R. Karr and T. M. Keinath, "Influence of particle size on sludge dewaterability," *Journal (Water Pollution Control Federation)*, vol. 50, no. 8, pp. 1911–1930, 1978.

[6] M. Abu-Orf and S. Dentel, "Effect of mixing on the rheological characteristics of conditioned sludge: Full-scale studies," *Water Science and Technology*, vol. 36, pp. 51–60, 12 1997.

[7] J. Baudez, F. Markis, N. Eshtiaghi, and P. Slatter, "The rheological behaviour of anaerobic digested sludge," *Water Research*, vol. 45, no. 17, pp. 5675–5680, 2011.

[8] V. Lotito, L. Spinosa, G. Mininni, and R. Antonacci, "The rheology of sewage sludge at different steps of treatment," *Water Science and Technology*, vol. 36, no. 11, pp. 79–85, 1997. Sludge Rheology Sludge Management.

[9] M. M. Abu-Orf and S. K. Dentel, "Effect of mixing on the rheological characteristics of conditioned sludge: full-scale studies," *Water Science and Technology*, vol. 36, pp. 51–60, 12 1997.

[10] N. Eshtiaghi, S. D. Yap, F. Markis, J.-C. Baudez, and P. Slatter, "Clear model fluids to emulate the rheological properties of thickened digested sludge," *Water Research*, vol. 46, no. 9, pp. 3014–3022, 2012.

[11] H. Versteeg and W. Malalasekera, *An Introduction to Computational Fluid Dynamics: The Finite Volume Method*. Pearson Education Limited, 2007.

[12] S. Patankar, *Numerical Heat Transfer and Fluid Flow*. Electro Skills Series, Hemisphere Publishing Corporation, 1980.

[13] L. Davidson, *Fluid mechanics, turbulent flow and turbulence modeling*. 2022.

[14] P. R. Spalart and C. L. Rumsey, "Effective inflow conditions for turbulence models in aerodynamic calculations," *AIAA Journal*, vol. 45, no. 10, pp. 2544–2553, 2007.

[15] T.-H. Shih, W. W. Liou, A. Shabbir, Z. Yang, and J. Zhu, "A new k- eddy viscosity model for high reynolds number turbulent flows," *Computers Fluids*, vol. 24, no. 3, pp. 227–238, 1995.

[16] P. R. Spalart, "Direct simulation of a turbulent boundary layer up to r = 1410," *Journal of Fluid Mechanics*, vol. 187, p. 61–98, 1988.

[17] F. Chen, "A survey of interface tracking methods in multi-phase fluid visualization.," vol. 19, pp. 11–19, 01 2010.

[18] M. Mikko, V. Taivassalo, and S. Kallio, "On the mixture model for multiphase flow," *VTT Publications*, vol. 288, 01 1996.

[19] T. Hibiki and M. Ishii, "One-dimensional drift-flux model and constitutive equations for relative motion between phases in various two-phase flow regimes," *International Journal of Heat and Mass Transfer*, vol. 46, no. 25, pp. 4935–4948, 2003.

[20] M. Ishii and T. Hibiki, *One-Dimensional Drift-Flux Model*, pp. 381–418. Boston, MA: Springer US, 2006.

[21] A. Y. Malkin and A. I. Isayev, "Introduction. rheology: Subject and goals," in *Rheology Concepts, Methods, and Applications (Second Edition)* (A. Y. Malkin and A. I. Isayev, eds.), pp. 1–8, Oxford: Elsevier, second edition ed., 2012.

[22] Y. Wang, E. Dieude-Fauvel, and S. Dentel, "Physical characteristics of conditioned anaerobic digested sludge - a fractal, transient and dynamic rheological viewpoint," *Journal of environmental sciences (China)*, vol. 23, pp. 1266–73, 08 2011.

[23] N. Inkson, D. Papoulias, M. Tandon, V. Reddy, and S. Lo, "An eulerian-eulerian formulation of suspension rheology using the finite volume method," *Journal of Non-Newtonian Fluid Mechanics*, vol. 245, pp. 38–48, 2017.

[24] Y. Li, J. Fu, Z. Geng, and H. Dong, "Cfd simulations of shear induced migration in pressure-driven flow with non-brownian suspensions," *International Journal of Multiphase Flow*, vol. 147, p. 103918, 2022.

[25] N. Corner-Walker, "The dry solids decanter centrifuge: Conveyor torque and differential," *Filtration and Separation*, vol. 37, 10 2000.

DEPARTMENT OF MECHANICS AND MARITIME SCIENCES
CHALMERS UNIVERSITY OF TECHNOLOGY
Gothenburg, Sweden 2022
www.chalmers.se

CHALMERS
UNIVERSITY OF TECHNOLOGY